Title: Bivalent mRNA booster encoding virus-like particles elicits potent polyclass receptor-binding domain antibodies in pre-vaccinated mice

Authors: Chengcheng Fan[1,7], Alexander A. Cohen[1,7], Kim-Marie A. Dam[2,7], Annie V. Rorick[1,3], Ange-Célia I. Priso Fils[1], Zhi Yang[1,4], Priyanthi N. P. Gnanapragasam[1], Luisa N. Segovia[1], Kathryn E. Huey-Tubman[1], Woohyun J. Moon[5], Paulo J.C. Lin[5], Pamela J. Bjorkman[1*], Magnus A. G. Hoffmann[2,6*]

Affiliations:

[1]Division of Biology and Biological Engineering, California Institute of Technology, Pasadena, CA 91125, USA

[2]Gladstone Institutes, San Francisco, CA 94158, USA

[3]Present address: Department of Biochemistry, University of Washington, Seattle, WA 98109, USA

[4]Present address: Department of Molecular and Cell Biology, University of California, Berkeley, Berkeley, CA 94720, USA

[5]Acuitas Therapeutics, Vancouver, BC, V6T 1Z3, CANADA

[6]Department of Medicine, University of California, San Francisco, CA 94143, USA

[7]These authors contributed equally

[*]To whom correspondence should be addressed: Email: bjorkman@caltech.edu, magnus.hoffmann@gladstone.ucsf.edu

Abstract

mRNA vaccines emerged as a leading vaccine technology during the COVID-19 pandemic. However, their sustained protective efficacies were limited by relatively short-lived antibody responses and the emergence of SARS-CoV-2 variants, necessitating frequent and variant-updated boosters. We recently developed the ESCRT- and ALIX-binding region (EABR) mRNA vaccine platform, which encodes engineered immunogens that induce budding of enveloped virus-like particles (eVLPs) from the plasma membrane, thereby resulting in presentation of immunogens on cell surfaces and eVLPs. Prior studies showed that spike (S)-EABR mRNA-LNP immunizations elicited enhanced neutralizing antibody responses against ancestral and variant SARS-CoV-2 compared with conventional S mRNA-LNP in naïve mice, but the effectiveness of S-EABR mRNA-LNP boosters in the context of pre-existing immunity has not been investigated. Here, we evaluated monovalent Wuhan-Hu-1 (Wu1) and bivalent (Wu1/BA.5) S-EABR mRNA-LNP boosters in mice pre-vaccinated with conventional Wu1 S mRNA-LNP. Compared to conventional S mRNA-LNP boosters, the EABR approach enhanced monovalent and bivalent mRNA-LNP booster-induced neutralizing responses against Omicron subvariants BA.1, BA.5, BQ.1.1, and XBB.1, with bivalent S-EABR mRNA-LNP consistently eliciting the highest titers. Epitope mapping of polyclonal antisera by deep mutational scanning revealed that bivalent S-EABR mRNA-LNP boosted diverse "polyclass" anti-receptor-binding domain (RBD) responses, suggesting balanced targeting of multiple RBD epitope classes. In contrast, monovalent S, bivalent S, and monovalent S-EABR mRNA-LNP boosters elicited less diverse polyclonal serum responses primarily targeting immunodominant RBD epitopes. Cryo-EM structures

46 demonstrated that bivalent mRNA immunizations promote S heterotrimer formation,
47 potentially enhancing bivalent S-EABR mRNA-LNP booster-induced antibody breadth
48 and polyclass epitope targeting by activating cross-reactive B cells through intra-S
49 crosslinking. These findings support the future design of bivalent or multivalent S-EABR
50 mRNA-LNP boosters as a promising strategy to confer broader, and therefore potentially
51 more durable, protection against emerging SARS-CoV-2 variants and other rapidly
52 evolving viruses.

53 **Introduction**

54 mRNA vaccines emerged as a leading platform for the rapid and scalable development
55 of effective vaccines during the COVID-19 pandemic[1]. Currently approved mRNA
56 vaccines encode the SARS-CoV-2 spike (S) trimer[2], the main target for neutralizing
57 antibodies (Abs) produced during natural infection[3]. S-encoding mRNAs formulated in
58 lipid nanoparticles (LNP) are taken up by cells, which promotes translation and cell
59 surface expression of S trimers to activate B cells[4]. Translation of mRNA-encoded S
60 protein within host cells also provides viral peptides for presentation on MHC class I
61 molecules, which are recognized by cytotoxic T cells[5,6].

62

63 Initial two-shot COVID-19 mRNA vaccination series became available in December 2020
64 after clinical studies demonstrated protection from severe disease after SARS-CoV-2
65 infection[7,8]. However, the durability of mRNA vaccine-induced immune protection was
66 limited by two factors. First, serum Ab levels contracted over several months[9]. Second,
67 SARS-CoV-2 variants acquired mutations in the S protein, which reduced their sensitivity
68 to vaccine-induced neutralizing Abs[10]. As a result, a third dose of the original mRNA
69 vaccine encoding the ancestral Wuhan-Hu-1 (Wu1) S protein was offered starting in fall
70 2021[11].

71

72 The emergence of the Omicron BA.1 variant in November 2021[12] sparked concern
73 because of its levels of substitution in S, especially in the receptor-binding domain (RBD),
74 resulting in effective evasion of Ab-mediated immunity[13,14] and increased rates of
75 symptomatic infections in previously vaccinated individuals[15,16]. Although undetectable

after the initial mRNA vaccine series, a third dose of the original mRNA vaccine elicited neutralizing Abs against BA.1, but BA.1 neutralizing titers were lower compared to titers against the ancestral Wu1 variant[17]. The subsequent emergence of Omicron subvariants such as BA.5, BQ.1.1, and XBB.1, which exhibited progressively reduced sensitivities to vaccine-induced neutralizing Abs[18], prompted the development of bivalent mRNA boosters, which included mRNAs encoding both the Wu1 and the BA.5 S proteins[19]. Preclinical and clinical studies found that bivalent boosters elicited modestly improved neutralizing Ab responses against Omicron subvariants compared to a fourth dose of the original monovalent vaccine[19-23], although some studies found no differences between monovalent and bivalent boosters following initial vaccination with the original Wu1 S-encoding mRNA vaccine[24,25]. Several studies[21,22,24,26-28] showed that the effectiveness of bivalent boosters was limited by immune imprinting, which occurs when prior exposure to an antigen shapes immunological responses to related antigens during subsequent exposures[29]. Instead of generating *de novo* Omicron-specific immune responses, bivalent boosters primarily activated pre-existing cross-reactive memory B cells from previous vaccinations and/or infections[26-28], leading to lower neutralizing activity against Omicron subvariants compared to the ancestral variant[21,22,24].

Continued development of updated boosters in response to emerging variants was slowed by the need for additional clinical testing, regulatory approvals, and adjustments to the manufacturing process. As a result, bivalent boosters became available in fall 2022, almost one year after the emergence of Omicron[30]. These challenges highlight the urgent need for innovative vaccine strategies that achieve more lasting immune protection

99 against rapidly-evolving viruses such as SARS-CoV-2, thereby reducing the need for
100 frequent and updated boosters.
101
102 We recently developed the ESCRT- and ALIX-binding region (EABR) mRNA vaccine
103 platform that combines features of mRNA and protein nanoparticle (NP) vaccines through
104 delivery of mRNA-encoded self-assembling enveloped virus-like particles (eVLPs)[31].
105 eVLP assembly is achieved by fusing a short EABR sequence to the cytoplasmic tail of
106 viral surface proteins, which recruits proteins from the Endosomal Sorting Complex
107 Required for Transport (ESCRT) pathway. Thus, EABR mRNA vaccines promote dual
108 presentation of S trimers on cell surfaces and eVLPs that bud from the plasma membrane.
109 Immunizations in mice showed that an EABR mRNA vaccine encoding a Wu1 SARS-
110 CoV-2 S elicited superior neutralizing Ab potency and breadth against ancestral and
111 Omicron SARS-CoV-2 variants compared to conventional mRNA and protein NP
112 vaccines[31]. Similar to conventional mRNA vaccines, the EABR mRNA vaccine also
113 induced potent T cell responses, consistent with the presence of S-specific cytotoxic T
114 cells[31]. These findings suggest that the EABR mRNA vaccine approach has the potential
115 to enhance monovalent or bivalent booster-induced Ab responses against Omicron
116 subvariants in the context of pre-existing immunity induced by prior vaccination, infection,
117 or both.
118
119 Here, we evaluated the ability of EABR mRNA boost immunogens to elicit potent and
120 broad humoral immune responses against SARS-CoV-2 variants in pre-vaccinated mice.
121 We demonstrate that the EABR mRNA vaccine approach improves monovalent and

122 bivalent booster-mediated neutralizing Ab responses against Omicron subvariants
123 compared to conventional mRNA boosters. Epitope mapping of polyclonal antisera further
124 showed that a bivalent EABR mRNA booster elicited a more diversified anti-RBD IgG
125 response than other tested boosting immunogens. These findings support the use of the
126 EABR mRNA vaccine platform for the design of effective boosters that could confer more
127 lasting protection against SARS-CoV-2 variants and potentially other rapidly-evolving
128 viruses. In addition, our work provides structural evidence that bivalent mRNA
129 immunizations promote heterotrimer formation, which could enhance activation of cross-
130 reactive B cells through intra-S crosslinking. These insights inform the future design of
131 bivalent or multivalent COVID-19 boosters and highlight the need for further investigation
132 into potentially beneficial effects of S heterotrimer formation on vaccine-induced immune
133 responses against trimeric viral Ss.
134
135 **Results**
136 To expand upon our previous characterizations of a monovalent SARS-CoV-2 S-EABR
137 mRNA vaccine[31], we evaluated the potential of the EABR mRNA vaccine approach for
138 monovalent and bivalent SARS-CoV-2 immunizations in pre-vaccinated mice. Four
139 cohorts of 10 BALB/c mice each initially received prime-boost intramuscular (IM)
140 vaccinations on days 0 and 28 with 2 μg of a conventional mRNA vaccine encoding the
141 ancestral S protein from the Wu1 variant, similar to the immunogens used in initially
142 approved COVID-19 mRNA vaccines (Wu1 S mRNA-LNP) (Fig. 1A-C). To simulate the
143 timing of the third available COVID-19 mRNA vaccine dose in humans, booster
144 immunizations were administered on day 230, nearly 7 months after the primary

145 vaccination series, with each cohort receiving a different boost immunogen (Fig. 1A-C).
146 Consistent with the COVID-19 booster that became available in fall 2021[11], cohort 1
147 received a third dose of 2 μg Wu1 S mRNA-LNP (Fig. 1B-C). To evaluate whether
148 formation of mRNA-encoded S-EABR eVLPs enhances booster immunogenicity in pre-
149 vaccinated mice, cohort 2 received 2 μg Wu1 S-EABR mRNA-LNP (Fig. 1B-C). Cohort 3
150 received a bivalent Wu1/BA.5 S mRNA-LNP booster (1 μg Wu1 S mRNA-LNP combined
151 with 1 μg BA.5 S mRNA-LNP), which resembled the COVID-19 booster that became
152 available in fall 2022[30] (Fig. 1B-C). Lastly, cohort 4 received a bivalent Wu1/BA.5 S-EABR
153 mRNA-LNP booster (1 μg Wu1 S-EABR mRNA-LNP combined with 1 μg BA.5 S-EABR
154 mRNA-LNP) to promote the formation of eVLPs that co-display Wu1 and BA.5 S trimers
155 (Fig. 1B-C). The Wu1 and BA.5 S-EABR constructs were designed as previously
156 described by fusing an endocytosis-preventing motif (EPM), a short Gly-Ser linker, and
157 an EABR sequence to the end of the cytoplasmic domain of Wu1 and BA.5 S trimers[31]
158 (Fig. S1A). The Wu1 and BA.5 S-EABR constructs induced similar levels of eVLP budding
159 in transiently transfected HEK293T cells (Fig. S1B).
160
161 Serum binding Ab responses were measured by enzyme-linked immunosorbent assay
162 (ELISA) four and 18 weeks after the primary vaccination series (days 56 and 154) and
163 two weeks after the booster immunizations (day 244). As previously observed, the initial
164 Wu1 S mRNA-LNP vaccinations elicited high binding Ab titers against soluble Wu1 S-6P
165 trimers (contain 6 proline substitutions to enhance expression and stability)[32], and as
166 expected, these titers were similar for all cohorts on day 56 (Fig. 1D). Robust binding Ab
167 responses were also detected for all cohorts against Omicron BA.5, BQ.1.1, and XBB.1

168 S-6P trimers on day 56 (Fig. 1E-G). On day 154, binding Ab levels against all variants
169 dropped slightly, which was consistent between cohorts (Fig. 1D-G). On day 244, all boost
170 immunogens increased binding Ab titers against Wu1, BA.5, BQ.1.1, and XBB.1 S-6P
171 trimers compared to titers measured on days 56 and 154, but no differences were
172 observed between cohorts for all timepoints (Fig. 1D-G).
173
174 **Bivalent S-EABR mRNA-LNP booster elicits potent Ab responses targeting**
175 **Omicron RBDs.**
176 We next evaluated the impact of the different boost immunizations on Ab responses
177 against the RBD, the primary target of neutralizing Abs[3]. The initial Wu1 S mRNA-LNP
178 prime-boost vaccinations elicited robust and similar Ab responses against the Wu1 RBD
179 for all cohorts on day 56 (Fig. 2A). The BA.5, BQ.1.1, and XBB.1 variants harbor multiple
180 RBD substitutions, particularly within the class 1 and 2 epitopes at the tip of the RBD[33]
181 (Fig. S2), promoting effective escape from neutralizing Abs[18]. Compared to Wu1 RBD
182 binding, Ab binding titers were weaker against the BA.5, BQ.1.1, and XBB.1 RBDs on day
183 56 (Fig. 2B-D). The robust Ab binding against the BA.5, BQ.1.1, and XBB.1 S trimers (Fig.
184 1E-G) in the absence of strong RBD responses was at least in part driven by potent
185 responses against the S2 stem region of S (residues 686-1213) (Fig. S3), which is
186 relatively conserved in SARS-CoV-2 variants[34] (Fig. S2). Similar to binding titers against
187 S-6P trimers (Fig. 1D-G), Wu1, BA.5, BQ.1.1, and XBB.1 RBD binding slightly dropped
188 on day 154 without statistically significant differences between cohorts (Fig. 2A-D). The
189 booster immunizations increased Wu1 RBD binding on day 244 compared to day 56 and
190 154 levels, but no differences were detected between the four boosting immunogens (Fig.

191 2A). In contrast, the bivalent Wu1/BA.5 S-EABR mRNA-LNP booster elicited the highest
192 BA.5, BQ.1.1, and XBB.1 RBD responses on day 244 (Fig. 2B-D), which were significantly
193 higher than Wu1 S mRNA-LNP booster-induced responses against BQ.1.1 RBD (p =
194 0.0499) (Fig. 2C) and narrowly failed to reach statistical significance compared to Wu1 S
195 mRNA-LNP booster-induced responses against BA.5 RBD (p = 0.07) (Fig. 2B).
196 Compared to baseline titers measured prior to boost immunizations on day 154, the
197 bivalent Wu1/BA.5 S-EABR mRNA-LNP immunization elicited significantly larger
198 increases in BA.5 RBD binding than the monovalent Wu1 S mRNA-LNP (p = 0.02) and
199 the bivalent Wu1/BA.5 S mRNA-LNP boosters (p = 0.01) (Fig. 2B), as well as significantly
200 larger increases in BQ.1.1 RBD binding than the Wu1 S mRNA-LNP booster (p = 0.002)
201 (Fig. 2C). While overall titers were similar on day 244, the monovalent Wu1 S-EABR
202 mRNA-LNP booster consistently induced larger increases in Ab binding to the BA.5,
203 BQ.1.1, and XBB.1 RBDs than the monovalent Wu1 S mRNA-LNP booster (Fig. 2B-D),
204 although these differences failed to reach statistical significance. The monovalent Wu1
205 and bivalent Wu1/BA.5 S mRNA-LNP boosters elicited similar binding titers against the
206 BA.5 and XBB.1 RBDs (Fig. 2B and D), but the bivalent booster induced slightly higher
207 responses and a larger increase compared to day 154 titers against BQ.1.1 RBD (not
208 statistically significant) (Fig. 2C). Overall, these results demonstrate that booster
209 immunizations with the bivalent Wu1/BA.5 S-EABR mRNA-LNP elicited the highest Ab
210 responses against Omicron RBDs in pre-vaccinated mice. Notably, post-boost Ab binding
211 against Omicron RBDs remained lower than binding titers against Wu1 RBD in all cohorts,
212 suggesting that booster responses were affected by immune imprinting induced by the
213 primary vaccination series.

214 **Bivalent S-EABR mRNA-LNP booster elicits higher neutralizing responses against**
215 **Omicron variants.**

216 The ability of boost immunogens to elicit neutralizing Ab responses in pre-vaccinated mice
217 was evaluated by in vitro pseudovirus neutralization assays[35,36]. The primary vaccination
218 series with Wu1 S mRNA-LNP elicited potent and consistent autologous geometric mean
219 neutralizing titers as assessed by half-maximal serum inhibitory dilution (ID_{50}) values
220 against Wu1 pseudovirus in all cohorts on day 56 (Fig. 3A; Table S1). Neutralizing activity
221 was >100-fold lower against the BA.5 variant and undetectable in most animals against
222 the BQ.1.1 and XBB.1 variants on day 56 for all cohorts (Fig. 3B-D; Table S1). On day
223 154, neutralizing titers against the Wu1 and BA.5 variants were consistent in all cohorts
224 and slightly lower compared to day 56 titers (Fig. 3A-B; Table S1). Neutralizing activity
225 against the BQ.1.1 and XBB.1 variants was undetectable in all but one animal on day 154
226 (Fig. 3C-D; Table S1). Booster immunizations on day 230 increased autologous
227 neutralizing titers against Wu1 pseudovirus on day 244 compared to day 154 in all cohorts
228 (Fig. 3A; Table S1). Monovalent Wu1 S mRNA-LNP and S-EABR mRNA-LNP
229 immunizations elicited the smallest and largest increases in Wu1 neutralization (4.2-fold
230 versus 6.6-fold), respectively. All boost immunogens elicited increased BA.5 neutralizing
231 activity on day 244 compared to day 56 and 154 titers (Fig. 3B; Table S1). Boosting with
232 monovalent Wu1 S-EABR mRNA-LNP induced 4.8-fold higher BA.5 neutralizing titers
233 than a third Wu1 S mRNA-LNP immunization, but this difference did not reach statistical
234 significance. Using the respective day 154 titers as baseline, the Wu1 S-EABR mRNA-
235 LNP booster induced a 23.8-fold increase in BA.5 neutralization on day 244 compared to
236 only a 6.3-fold increase detected after boosting with Wu1 S mRNA-LNP (not statistically

237 significant) (Fig. 3B; Table S1). Compared to day 56 baseline titers, the Wu1 S-EABR
238 mRNA-LNP booster induced a significantly higher increase in BA.5 neutralization on day
239 244 than the conventional Wu1 S mRNA-LNP booster (16.2-fold versus 3.1-fold; p =
240 0.048) (Fig. S4; Table S1). The Wu1 S-EABR mRNA-LNP booster also elicited 3.4-fold
241 higher neutralizing responses than the Wu1 S mRNA-LNP booster against the Omicron
242 BA.1 variant on day 244 (p = 0.03) (Fig. S5). Based on day 154 titers, boosting with
243 monovalent Wu1 S-EABR mRNA-LNP induced significantly higher increases in BA.1
244 neutralization compared to monovalent Wu1 S mRNA-LNP (8.8-fold versus 2.5-fold; p =
245 0.009) (Fig. S5). Interestingly, the monovalent Wu1 S-EABR mRNA-LNP and the bivalent
246 Wu1/BA.5 S mRNA-LNP boosters elicited similar BA.5 neutralizing responses on day 244
247 (Fig. 3B; Table S1), suggesting that the EABR mRNA vaccine approach might reduce the
248 need for updating boost immunogens to achieve robust Ab responses against emerging
249 SARS-CoV-2 variants. The highest BA.5 neutralizing titers were elicited by the bivalent
250 Wu1/BA.5 S-EABR mRNA-LNP booster, which were 12.3-fold higher than titers induced
251 by the monovalent Wu1 S mRNA-LNP booster (p = 0.02) and 2.4-fold higher than titers
252 induced by the bivalent Wu1/BA.5 S mRNA-LNP booster (not statistically significant).
253 Based on titers measured on day 154, the Wu1/BA.5 S-EABR mRNA-LNP booster
254 induced a 67-fold increase in BA.5 neutralization, which was significantly higher than the
255 increase elicited by boosting with monovalent Wu1 S mRNA-LNP (p = 0.003).
256
257 While the BA.5 neutralizing activity induced by the monovalent Wu1 S and S-EABR
258 mRNA-LNP boosters can likely be attributed to cross-neutralizing Abs that neutralize both
259 the Wu1 and BA.5 variants, it is possible that the bivalent Wu1/BA.5 S and S-EABR

260 mRNA-LNP boosters also elicited *de novo* strain-specific Abs that neutralize BA.5 but not
261 Wu1. Day 244 serum samples from mice that received bivalent Wu1/BA.5 S or S-EABR
262 mRNA-LNP boosters were depleted of Abs that bind to Wu1 RBD. Sera were passaged
263 over a column presenting either a mock protein (HIV-1 gp120) as a control or the Wu1
264 RBD to remove cross-neutralizing anti-RBD Abs while retaining BA.5 RBD-specific Abs.
265 Following depletions, residual neutralization activity was measured against the BA.5
266 variant. Interestingly, Wu1 RBD depletion resulted in 17- and 36-fold lower geometric
267 mean neutralizing titers compared to mock depletion for the bivalent Wu1/BA.5 S and S-
268 EABR mRNA-LNP boosters, respectively (Fig. S6). In both cohorts, BA.5 neutralizing
269 titers in all but two mice dropped below ID_{50} values of 1:120 following Wu1 RBD depletion,
270 consistent with the neutralizing activity in these samples being primarily driven by cross-
271 neutralizing Abs targeting the RBD induced by the primary vaccination series. The potent
272 residual neutralizing activity observed in two mice in each cohort after Wu1 RBD depletion
273 implies either the presence of boost-induced *de novo* BA.5-specific RBD Abs or
274 neutralizing non-RBD Abs that target another region of S, e.g., the N-terminal domain[37]
275 or S2[34].
276
277 Booster immunizations had less pronounced effects on neutralization activity against the
278 BQ.1.1 and XBB.1 variants. Against BQ.1.1 pseudovirus, the bivalent Wu1/BA.5 S-EABR
279 mRNA-LNP booster elicited the most potent neutralizing activity on day 244, which was
280 significantly higher than responses induced by a third immunization with the monovalent
281 Wu1 S mRNA-LNP booster ($p = 0.0495$) (Fig. 3C; Table S1). The monovalent Wu1 S-
282 EABR mRNA-LNP and bivalent Wu1/BA.5 S mRNA-LNP boosters elicited 1.8- and 2.5-

283 fold higher BQ.1.1 titers than the monovalent Wu1 S mRNA-LNP booster, respectively,
284 the latter of which narrowly failed to reach statistical significance ($p = 0.07$). Based on day
285 154 BQ.1.1 neutralizing titers, the monovalent Wu1 S mRNA-LNP and bivalent Wu1/BA.5
286 S-EABR mRNA-LNP boosters induced the smallest and largest increases in neutralizing
287 activity on day 244, respectively (1.4-fold versus 4.7-fold; $p = 0.0495$). The monovalent
288 Wu1 S-EABR mRNA-LNP and bivalent Wu1/BA.5 S mRNA-LNP boosters elicited 2.4-
289 and 3.4-fold increases in neutralizing BQ.1.1 titers, respectively. Notably, day 244
290 neutralizing titers against BQ.1.1 were substantially lower than BA.5 neutralizing titers for
291 all boost immunogens (Fig. 3B-C; Table S1), consistent with previous reports[18,38]. Notably,
292 Ab binding responses against the BA.5 and BQ.1.1 RBDs were similar (Fig. 2B-C),
293 implying that RBD binding responses are not always predictive of neutralizing activity
294 against Omicron subvariants.
295
296 Neutralizing responses against the XBB.1 variant were slightly lower than titers against
297 BQ.1.1 pseudovirus (Fig. 3D; Table S1). Once again, the bivalent Wu1/BA.5 S-EABR
298 mRNA-LNP booster elicited the highest XBB.1 neutralizing titers, which were 2.1-fold
299 higher than titers induced by the monovalent Wu1 S mRNA-LNP booster (not statistically
300 significant). Based on day 154 titers, the monovalent Wu1 and bivalent Wu1/BA.5 S-
301 EABR mRNA-LNP boosters increased XBB.1 neutralization by 2.5- and 3.2-fold,
302 respectively, while conventional monovalent and bivalent S mRNA-LNP boosters only
303 induced 1.5- and 2.2-fold increases, respectively.
304

305 Notable differences were also observed in the number of mice in each cohort that reached
306 robust neutralizing titers (defined as ID_{50}s exceeding 1:100) against Omicron subvariants
307 following booster immunizations, titers that are likely important for the prevention of
308 symptomatic infections[39]. The primary vaccination series with Wu1 S mRNA-LNP elicited
309 robust neutralizing titers against the Wu1 variant in all mice on day 56 (Fig. 3E). However,
310 the initial Wu1 S mRNA-LNP vaccinations elicited robust titers in only 6 to 8, 1 to 3, and
311 0 to 2 of 10 mice against the BA.5, BQ.1.1, and XBB.1 variants on day 56, respectively.
312 On day 154, ID_{50}s over 1:100 were measured for 3 to 5 mice in each cohort against BA.5,
313 but for none of the animals against BQ.1.1 and XBB.1. While a third immunization with
314 Wu1 S mRNA-LNP induced robust titers against BA.5 in only 8 of 10 mice on day 244,
315 the monovalent Wu1 S-EABR mRNA-LNP booster induced robust titers against BA.5 in
316 all 10 mice, including the 4 mice that did not have detectable BA.5 neutralizing activity on
317 day 56 (Fig. 3E). As expected, robust neutralizing titers against the BA.5 variant were
318 also observed in all mice that received the bivalent Wu1/BA.5 S or S-EABR mRNA-LNP
319 boosters. Against the BQ.1.1 and XBB.1 variants, a third immunization with Wu1 S
320 mRNA-LNP induced robust neutralizing titers in only 2 and 3 mice, respectively (Fig. 3E).
321 In comparison, the bivalent Wu1/BA.5 S-EABR mRNA-LNP booster induced ID_{50}s over
322 1:100 in 7 and 6 mice against the BQ.1.1 and XBB.1 variants, respectively.
323
324 Overall, these results demonstrate that the EABR mRNA vaccine approach improves the
325 neutralizing activity against Omicron subvariants induced by monovalent and bivalent
326 boost immunogens in pre-vaccinated mice.
327

328 **Bivalent S-EABR mRNA-LNP booster induces polyclass Ab responses.**

329 Several distinct Ab-binding epitopes have been defined on RBDs, including the variable
330 class 1 and 2 RBD epitopes and the more conserved class 3, 4, 1/4, and 5 RBD
331 epitopes[33,40,41] (Fig. S2). We determined which RBD epitopes were targeted by booster-
332 induced Abs in pre-vaccinated mice using deep mutational scanning (DMS) of yeast
333 display libraries derived from Wu1[42] and XBB.1.5 RBDs[43]. In previous studies, we showed
334 that equimolar mixtures of monoclonal Abs targeting distinct RBD epitopes produced less
335 pronounced DMS escape peaks, which we defined as a polyclass Ab response[44]. This
336 suggests that polyclonal serum that includes roughly equal distributions of Abs targeting
337 multiple classes of RBD epitopes would exhibit relatively flat DMS profiles, while more
338 defined DMS escape peaks would be observed for less diverse polyclonal serum
339 responses containing Abs that primarily target particular RBD epitopes[44]. For this study,
340 we used DMS escape fractions to define polyclass responses. Escape fractions for each
341 RBD mutation range from 0 (no cells with this mutation are sorted into the serum Ab
342 escape bin) to 1 (all cells with this mutation are sorted into the serum Ab escape bin)[45].
343 Total escape peaks represent the sum of escape fractions for all mutations at a specific
344 site[45]. DMS profiles with total escape peaks below 0.5 at all sites were classified as
345 polyclass responses. In contrast, DMS profiles with total escape peaks of 0.5-1, 1-2, or
346 above 2 at one or more sites were classified as weak, moderate, or strong escape profiles,
347 respectively, indicating weak, moderate, or strong targeting of particular RBD epitopes
348 (Table S2). DMS was performed for 6 serum samples for each cohort, which were
349 selected based on XBB.1 neutralization activity (1st, 2nd, 3rd, 5th, 6th, and 10th best

350 neutralizer from each cohort). For the Wu1 RBD library, only 5 DMS profiles were obtained
351 due to poor sequencing quality for one sample in each cohort.
352
353 Against the Wu1 RBD library, immunizations with the monovalent Wu1 S and S-EABR
354 mRNA-LNP boosters or the bivalent Wu1/BA.5 S mRNA-LNP booster resulted in DMS
355 profiles consistent with moderate targeting of the variable class 2 epitope primarily
356 inducing escape at RBD residue 484 (Fig. 4A-B). The bivalent Wu1/BA.5 S mRNA-LNP
357 booster also elicited weak to moderate responses that mapped to the variable class 1
358 and class 3 RBD epitopes. In contrast, the bivalent Wu1/BA.5 S-EABR mRNA-LNP
359 booster DMS profiles were consistent with polyclass Ab induction, suggesting a more
360 diverse response targeting multiple RBD epitopes (Fig. 4A-B). Notably, samples from 4
361 out of 5 mice in this cohort exhibited polyclass DMS profiles, whereas moderate to strong
362 escape fractions for class 1, 2, or 3 epitopes were observed in 3-4 mice in each of the
363 other cohorts (Fig. S7; Table S2).
364
365 As expected, no class 1 and 2 DMS profiles were observed against the XBB.1.5 RBD
366 library[43] since these epitopes are highly substituted in Omicron subvariants (Fig. S2). All
367 booster immunizations induced strong class 5 escape peaks targeting RBD residues 352,
368 357, 396, and 468 (Fig. 4C-D). Importantly, the bivalent Wu1/BA.5 S-EABR mRNA-LNP
369 booster induced a less pronounced overall class 5 profile than the other boost
370 immunogens, which was primarily driven by a strong class 5 response observed in a
371 single animal in this cohort (Fig. S8; Table S2). The other mice that received the bivalent
372 Wu1/BA.5 S-EABR mRNA-LNP booster exhibited polyclass or weak to moderate

373 responses against class 4 and 5 epitopes. In contrast, strong class 5 profiles were
374 detected in 4-5 mice in cohorts that received the monovalent Wu1 S or S-EABR mRNA-
375 LNP boosters or the bivalent Wu1/BA.5 S mRNA-LNP booster (Fig. S8; Table S2).
376 Overall, these results suggest that the bivalent Wu1/BA.5 S-EABR mRNA-LNP booster
377 induced a more diversified polyclass Ab response that likely contributed to the higher
378 neutralizing activity observed against Omicron subvariants, which could result in more
379 effective recognition of future variants.
380
381 **Co-expression of Wu1 and BA.5 S results in heterotrimer formation.**
382 The results from this and previous studies[19-22] demonstrated that bivalent booster
383 immunizations improve the potency and breadth of Ab responses against Omicron
384 subvariants compared to monovalent boosters. Serum depletion assays also showed that
385 the BA.5 neutralizing activity elicited by the bivalent Wu1/BA.5 S and S-EABR mRNA-
386 LNP boosters was primarily driven by cross-reactive Abs that bind to the Wu1 and BA.5
387 RBDs (Fig. S6). Preferential activation of cross-reactive B cells could be achieved through
388 co-display of Wu1 and BA.5 S trimers on the surface of a cell and/or an eVLP (Fig. 1C),
389 which could result in inter-S crosslinking between cross-reactive B cell receptors (BCRs)
390 and neighboring homotrimeric Wu1 and BA.5 S trimers (Fig. S9). As an additional
391 mechanism for bivalent booster-induced activation of cross-reactive B cells, we
392 hypothesized that co-expression of ancestral Wu1 and Omicron S in the same cell could
393 result in the formation of S heterotrimers consisting of Wu1 and Omicron S protomers and
394 could promote intra-S crosslinking, i.e., simultaneous binding of cross-reactive BCRs to
395 two neighboring RBDs within the same S trimer (Fig. S9). We previously postulated that

396 intra-S crosslinking is possible for several anti-RBD IgGs based on modeling of intact IgG
397 coordinates into single-particle cryo-electron microcopy (cryo-EM) structures of fragment
398 antigen-binding (Fab)-S complexes[33,40], and intra-S crosslinking was observed in EM
399 studies of IgG-S trimer complexes[46]. However, it is currently unknown whether co-
400 expression of Wu1 and Omicron Ss induces heterotrimerization, and if so, whether
401 heterotrimer formation affects the overall structure of the S ectodomain and influences
402 bivalent booster-induced immune responses.
403
404 To investigate whether S heterotrimers could form with different S protomers, we
405 designed 6P versions (contain 6 proline substitutions to enhance expression and
406 stability)[32] of Wu1/BA.1 and Wu1/BA.1/Delta soluble heterotrimer Ss (HT2 and HT3,
407 respectively) by co-transfection with specific C-terminally-tagged constructs. HT2 was
408 generated by co-transfecting StrepII-tagged Wu1 S and His-tagged BA.1 S, while HT3
409 was generated using StrepII-tagged Wu1 S, His-tagged BA.1 S, and D7324[47]-tagged
410 Delta S (Fig. 5A). Each heterotrimer was subsequently purified using sequential affinity
411 purification specific to each tag, confirming the inclusion of distinct protomers in the
412 purified heterotrimers (Fig. 5A).
413
414 HT2 and HT3 S proteins were then evaluated using single-particle cryo-electron
415 microscopy (cryo-EM) to determine whether heterotrimeric Ss resembling their
416 homotrimeric counterparts were formed. To ensure that C-terminal tags did not disrupt
417 the formation of trimers, we included the following controls: (1) three homotrimers with
418 single tags (StrepII-tagged Wu1 S, His-tagged BA.1 S, and D7324-tagged Delta S), and

419 (2) a homotrimer comprised of His- and StrepII-tagged protomers (Wu1-His/Wu1-StrepII).
420 Single-particle cryo-EM analysis confirmed that all control S proteins formed trimers,
421 indicating that C-terminal tags did not disrupt trimerization (Fig. S10). Because most of
422 the EM constructions for homotrimeric S controls exhibited preferred orientations, we
423 determined overall conformational states (Fig. 5) for the control structures but did not fit
424 atomic models. Structural analysis also revealed trimerized HT2 and HT3 Ss (Fig. 5B-C,
425 Fig. S10). Although atomic models could not be built for the HT2 and HT3 trimer
426 reconstructions because the identities of individual protomers (Wu1 or BA.1 for HT2, and
427 Wu1, BA.1, or Delta for HT3) could not be conclusively determined at relatively low
428 resolution, the EM densities of S heterotrimers and control homotrimers showed no major
429 conformational differences in domain organization (Fig. 5B-C, Fig. S10). As previously
430 seen in SARS-CoV-2 S trimer structures[48,49], we observed two trimer populations in all
431 datasets—one with all three RBDs in the 'down' conformation and one with a single RBD
432 in an 'up' conformation (Fig. 5D). These data demonstrate heterotrimeric S formation for
433 soluble forms of SARS-CoV-2 S proteins. This result suggests that the bivalent S or S-
434 EABR mRNA-LNP boost immunogens likely induce heterotrimerization, which could
435 promote activation of cross-reactive B cells through intra-S cross-linking, a potential
436 mechanism warranting further investigation.
437

438 **Discussion**

439 The EABR mRNA vaccine platform delivers mRNA encoding engineered immunogens
440 that induce budding of enveloped virus-like particles (eVLPs) from the plasma membrane
441 to promote presentation of immunogens on cell surfaces and eVLPs[31]. This approach

442 elicited superior neutralizing Ab responses in naïve mice compared to a conventional
443 mRNA vaccine against original and variant SARS-CoV-2[31]. However, the majority of the
444 human population has already mounted immune responses against SARS-CoV-2 through
445 prior vaccinations, natural infections, or a combination of both. Here, we demonstrate that
446 the EABR mRNA vaccine approach improves humoral immune responses elicited by
447 monovalent and bivalent mRNA-LNP booster immunizations against Omicron subvariants
448 in pre-vaccinated mice.
449
450 The possibility of receiving a third dose of the original COVID-19 mRNA vaccine in fall
451 2021[11] coincided with the emergence of the Omicron variants in November 2021[12]. These
452 variants had acquired many substitutions, especially in the RBD, which allowed efficient
453 evasion of Ab-mediated immunity[13,14] and rapid global spread. Similar to the effects of a
454 third vaccination in humans[17], a third immunization in pre-vaccinated mice with a
455 monovalent Wu1 S mRNA-LNP booster elicited modest neutralizing activity against the
456 early Omicron variants BA.1 and BA.5. However, addition of an EABR sequence[31] to the
457 boosting immunogen resulted in higher Ab neutralizing titers against BA.1 and BA.5,
458 suggesting that a monovalent Wu1 S-EABR booster could have promoted enhanced
459 protection against early Omicron variants. Importantly, the monovalent Wu1 S-EABR
460 mRNA-LNP booster elicited similar neutralizing responses against the BA.5, BQ.1.1, and
461 XBB.1 subvariants compared to the conventional bivalent S mRNA-LNP booster that
462 contained both Wu1 and BA.5 S immunogens.
463

464 While updating of mRNA vaccines can be done relatively quickly, the development,
465 clinical testing, approval, and large-scale manufacturing of a bivalent booster that
466 includes updated immunogens based on new circulating variants cannot be accomplished
467 fast enough to keep up with viral evolution during a global pandemic such as COVID-19.
468 Indeed, the Wu1/BA.5 bivalent booster became available in fall 2022, almost one year
469 after the emergence of Omicron variants[30]. The results reported here suggest that the
470 EABR mRNA vaccine approach presents a potential solution that could reduce the need
471 for frequent development of updated COVID-19 boosters and potentially future pandemic
472 viruses. Combined with our previous finding that an initial two-shot vaccination series with
473 a Wu1 S-EABR mRNA-LNP immunogen elicited substantially higher neutralizing activity
474 against Omicron variants than conventional Wu1 S mRNA-LNP immunizations in naïve
475 mice[31], our results demonstrate that the EABR mRNA vaccine approach has the potential
476 to induce more effective and lasting humoral immunity against emerging SARS-CoV-2
477 variants and represents a promising platform for future pandemic preparedness.
478
479 Clinical studies showed that the bivalent COVID-19 mRNA booster outperformed the
480 monovalent mRNA booster in terms of preventing symptomatic illness, hospitalizations,
481 and deaths when administered as a fourth dose in humans[30,50]. Consistent with other
482 studies[19-23], the bivalent conventional and EABR-based boosters evaluated in this study
483 elicited higher neutralizing responses against Omicron subvariants than their monovalent
484 counterparts in pre-vaccinated mice, although improvements were relatively modest.
485 However, the bivalent Wu1/BA.5 S-EABR mRNA-LNP booster consistently elicited the
486 highest RBD binding and neutralizing titers against all tested Omicron subvariants and

487 induced robust neutralizing responses in the highest number of animals against the
488 BQ.1.1 and XBB.1 variants that are particularly difficult to neutralize[18,38] These results
489 highlight that the EABR mRNA vaccine approach and the bivalent booster strategy work
490 synergistically to induce more effective humoral immune responses.
491
492 In addition to eliciting the most potent neutralizing responses against Omicron
493 subvariants, the bivalent Wu1/BA.5 S-EABR mRNA-LNP booster also induced distinct
494 DMS signatures compared to the other boost immunogens, consistent with differences in
495 epitope mapping of polyclonal anti-RBD Ab responses. While the monovalent Wu1 S and
496 S-EABR mRNA-LNP and the bivalent Wu1/BA.5 S mRNA-LNP boosters elicited
497 predominantly class 1 and class 2 responses against Wu1 RBD and strong class 5
498 responses against XBB.1.5 RBD, boost immunizations with bivalent Wu1/BA.5 S-EABR
499 mRNA-LNP elicited polyclass serum Ab responses against Wu1 RBD and mostly
500 polyclass or moderate polyclass class 4 and class 5 responses against XBB.1.5 RBD.
501 These results imply that combining the bivalent booster strategy with the EARB mRNA
502 vaccine approach elicited a more diversified Ab response, resulting in simultaneous and
503 balanced targeting of multiple RBD epitopes. A more diverse anti-RBD Ab response might
504 be desirable as viral immune evasion would require mutations in multiple sites, including
505 the more conserved class 4 and 5 RBD epitopes. As a potential mechanism for the more
506 frequent induction of polyclass-like Ab responses, we hypothesize that EABR eVLP
507 formation promotes close proximity of Wu1 and BA.5 S trimers on densely-coated eVLPs,
508 consistent with cryo-electron tomography imaging of purified eVLPs showing that the
509 density of S trimers was equivalent or higher than on SARS-CoV-2 virions (20-40 S

510 trimers on 40-60 nm diameter eVLPs)[31]. The high density of co-displayed Wu1 and BA.5
511 S trimers on eVLPs should facilitate inter-S crosslinking by B cell receptors that recognize
512 epitopes that are conserved between Wu1 and BA.5 S trimers, leading to preferential
513 activation of cross-reactive B cells. By comparison, conventional bivalent mRNA booster-
514 mediated co-expression of Wu1 and BA.5 S trimers could result in lower S trimer density
515 on cell surfaces that are crowded with endogenous membrane proteins, which could
516 prevent efficient inter-S crosslinking.
517
518 As an additional mechanism for bivalent booster-induced preferential activation of cross-
519 reactive B cells, we provide evidence that co-expression of ancestral and Omicron S
520 results in heterotrimer formation that could promote intra-S crosslinking, i.e.,
521 simultaneous binding of both Fabs of a cross-reactive BCR to neighboring RBDs within
522 the same S trimer. We previously postulated that intra-S crosslinking is possible for
523 several anti-RBD Abs that target various RBD epitopes based on modeling of intact IgG
524 structures onto cryo-EM structures of Fab-S complexes[33,40]. The conventional mRNA-
525 and the EABR mRNA-based bivalent boost immunogens should promote similar degrees
526 of heterotrimerization and intra-S crosslinking. While our RBD serum depletion assays
527 showed that both bivalent boosters primarily elicited cross-neutralizing Abs that bind to
528 the Wu1 and BA.5 RBDs, only the EABR mRNA-based bivalent booster induced
529 predominantly polyclass DMS signatures. Thus, it is possible that the diversification of the
530 anti-RBD Ab response observed for the bivalent EABR mRNA booster was primarily
531 driven by inter-S crosslinking possibly in conjunction with intra-S crosslinking. Future
532 studies are needed to investigate the impact of inter- and intra-S crosslinking on the

533 activation of cross-reactive B cells and to evaluate whether the EABR mRNA vaccine
534 approach can improve other types of bivalent and multivalent vaccines.
535
536 Although our results highlight the potential of the EABR mRNA vaccine approach in the
537 context of pre-existing immunity, we observed that monovalent and bivalent EABR mRNA
538 booster-induced humoral immune responses were still largely dictated by immunological
539 imprinting resulting from the initial vaccination series. Post-boost BA.5 neutralizing
540 responses were roughly an order of magnitude lower than Wu1 neutralization titers, even
541 for bivalent boosters that included BA.5 S immunogens. In addition, despite eliciting
542 consistent polyclass anti-RBD Ab responses, bivalent EABR mRNA booster-induced
543 neutralizing activity against the BQ.1.1 and XBB.1 variants dropped over 10-fold
544 compared to BA.5 neutralization. Notably, Ab binding responses to BQ.1.1 and XBB.1
545 RBDs were similar compared to BA.5 RBD binding for all boost immunogens. This
546 discrepancy between RBD binding responses and neutralization titers indicates that only
547 a relatively small fraction of binding Abs has neutralizing activity and/or the Abs still bind
548 to the BQ.1.1 and XBB.1 RBDs, but fail to effectively prevent interactions with ACE2 on
549 the surface of target cells. The initial two-shot COVID-19 mRNA vaccination series and
550 all booster immunizations elicited potent binding responses against the S2 region, which
551 is relatively conserved among SARS-CoV-2 variants[34]. Consistent with previous reports[51],
552 our depletion studies showed that anti-S2 Abs had little impact on virus neutralization,
553 which was instead predominantly driven by anti-RBD Abs. However, anti-S2 Abs could
554 still provide valuable immune protection against symptomatic Omicron infections through
555 Fc-mediated effector functions[52]. In addition, mRNA vaccines induce potent cytotoxic T

556 cell responses that cross-recognize Omicron variants[53] and reduce COVID-19 disease
557 severity[54].
558
559 Taken together, our results demonstrate that the EABR mRNA vaccine approach
560 improves monovalent and bivalent booster-mediated humoral immune responses against
561 Omicron subvariants in pre-vaccinated mice. DMS epitope mapping studies further
562 showed that the bivalent EABR mRNA booster elicited a more diversified anti-RBD Ab
563 response than all other tested boost immunogens. Our work also provides evidence that
564 bivalent mRNA booster immunizations promote heterotrimer formation, which could
565 activate cross-reactive B cells through intra-S crosslinking. Despite these advances,
566 future work is needed to develop booster strategies that overcome immunological
567 imprinting more effectively and confer lasting immunity against emerging variants.
568
569 **Limitations of the study**
570 Due to the substantial time required to conduct immunization studies in pre-vaccinated
571 mice, this proof-of-concept study to evaluate the potential of EABR-modified boosters in
572 the context of pre-existing immunity was performed using outdated SARS-CoV-2 variants.
573 Future studies are needed to assess EABR booster responses against currently
574 circulating variants. While the monovalent Wu1 S-EABR mRNA-LNP booster elicited
575 robust improvements in neutralization titers against BA.1 and BA.5 compared to the
576 conventional Wu1 S mRNA-LNP booster, consistent with previously reported results in
577 naïve mice[31], only modest and statistically non-significant increases were observed for
578 later Omicron variants, such as BQ.1.1 and XBB.1. Moreover, although the bivalent

579 Wu1/BA.5 S-EABR mRNA-LNP booster consistently induced the highest neutralizing
580 titers across all tested variants, these increases were statistically significant only relative
581 to the conventional monovalent Wu1 S mRNA-LNP and not the bivalent Wu1/BA.5 S
582 mRNA-LNP booster. Larger mouse cohorts could have increased the statistical power of
583 the study, such that the observed trends might have reached statistical significance.
584 Another factor contributing to the relatively modest improvements elicited by the
585 monovalent and bivalent EABR boosters against BQ.1.1 and XBB.1 was the generally
586 low levels of neutralizing responses observed against these variants. Although the low
587 neutralization activity against BQ.1.1 and XBB.1 was likely the result of immune imprinting
588 caused by the initial vaccination series, addition of more cohorts might have excluded the
589 possibility that the ancestral Wu1 S immunogen is more immunogenic than the Omicron
590 BA.5 S immunogen, e.g., three immunizations with monovalent BA.5 S or bivalent
591 Wu1/BA.5 S mRNA-LNP. However, this is unlikely since prior studies reported that
592 ancestral and Omicron S immunogens are similarly immunogenic[19,55,56]. Finally, it
593 remains unclear why the polyclonal RBD epitope–targeting response elicited by the
594 bivalent Wu1/BA.5 S-EABR mRNA-LNP booster translated into only modest gains in
595 neutralizing activity against Omicron variants. It is possible that a longer post-boost follow-
596 up period or an additional booster incorporating an XBB.1 S immunogen would have
597 revealed further maturation and expansion of these responses, and thereby additional
598 benefits of the bivalent EABR booster.
599
600
601

602 **Methods**

603 **Design of EABR constructs**

604 SARS-CoV-2 S-EABR constructs were designed as described[31]. The EABR domain
605 (residues 160-217) of the human CEP55 protein was fused to the C-terminus of the
606 SARS-CoV-2 S protein obtained from the Wu1 (GenBank: QTA38991.1) or BA.5
607 (GenBank: UPP14409.1) variants separated by a 4-residue $(Gly)_3Ser$ (GS) linker (Fig.
608 S1A). These constructs contained the native furin cleavage site, 2P stabilizing
609 mutations[57], and the C-terminal 21 residues were truncated to remove an endoplasmic
610 reticulum retention signal[58]. The D614G substitution[59], naturally present in BA.5, was
611 inserted into Wu1 S and S-EABR constructs. To prevent endocytosis and enhance the
612 cell surface expression of S-EABR constructs, an EPM (residues 243-290 of mouse
613 FcgRII-B1)[31,60] was inserted upstream of the 4-residue Gly-Ser linker and the EABR
614 domain as described[31] (Fig. S1A).

615

616 **In vitro transfection**

617 To verify that the designed constructs induce eVLP budding, HEK293T were transiently
618 transfected with DNA plasmids encoding Wu1 or BA.5 S-EABR using Fugene HD
619 (Promega). After 48 hours, transfected cell supernatants were harvested, and eVLPs
620 were purified by ultracentrifugation on a 20% sucrose cushion as described[31]. The purified
621 eVLP fractions were 3-fold serially diluted in 0.1 M $NaHCO_3$ pH 9.6, directly coated onto
622 Costar high binding 96-well plates (Corning), and eVLP-associated S protein levels were
623 quantified by ELISA. After 1 hour blocking in Tris-buffered saline with 0.1% TWEEN 20
624 (TBS-T) and 3% bovine serum albumin (BSA) (TBS-T/3% BSA) at room temperature, the

625 monoclonal anti-S2 Ab S2P6[61] was diluted to a concentration of 5 µg/mL in TBS-T/3%
626 BSA and added to plates for 1 hour at room temperature. After washing with TBS-T, HRP-
627 conjugated goat anti-human IgG (2015-05; SouthernBiotech) was diluted 1:8,000 in TBS-
628 T/3% BSA and added to plates for 30 min at room temperature. After washing with TBS-
629 T, plates were developed using 1-Step™ Ultra TMB-ELISA Substrate Solution (Thermo
630 Fisher Scientific) and absorbance was measured at 450 nm.
631
632 **mRNA synthesis**
633 Codon-optimized mRNAs encoding Wu1 S, Wu1 S-EABR, BA.5 S, and BA.5 S-EABR
634 constructs were synthesized by RNAcore (https://www.houstonmethodist.org/research-
635 cores/rnacore/) using proprietary manufacturing protocols as described[31]. In brief,
636 mRNAs were synthesized by T7 RNA polymerase-mediated in vitro transcription using
637 DNA templates encoding the immunogen open reading frame flanked by 5′ and 3'
638 untranslated regions and terminated by an encoded polyA tail. CleanCap 5' cap structures
639 (TriLink) were co-transcriptionally incorporated into the 5′ end. Uridine was completely
640 substituted with N1-methyl-pseudouridine to lower immunogenicity[62]. mRNAs were
641 purified by oligo-dT affinity purification and high-performance liquid chromatography
642 (HPLC) to remove double-stranded RNA contaminants[63]. Purified mRNAs were stored
643 at –80 °C.
644
645 **LNP encapsulation of mRNAs**
646 Purified mRNAs were formulated in LNP as described[31,64]. In brief, 1,2-distearoyl-*sn*-
647 glycero-3-phosphocholine, cholesterol, a PEG lipid, and an ionizable cationic lipid

648 dissolved in ethanol were rapidly mixed with an aqueous acidic solution containing the
649 mRNAs using an in-line mixer. The ionizable lipid and LNP composition are described in
650 the international patent application WO2017075531(2017). The post in-line solution was
651 dialyzed with PBS to remove ethanol and displace the acidic solution. Subsequently,
652 mRNA-LNP were measured for size (60-65 nm) and polydispersity (PDI < 0.075) by
653 dynamic light scattering (Malvern Nano ZS Zetasizer). The encapsulation efficiencies
654 were >97% as measured by the Quant-iT Ribogreen Assay (Invitrogen).
655
656 **Immunizations**
657 All animal procedures in this study were performed in compliance with the U.S.
658 Department of Agriculture's (USDA) Animal Welfare Act (9 CFR Parts 1, 2, and 3); the
659 Guide for the Care and Use of Laboratory Animals (Institute of Laboratory Animal
660 Resources, National Academy Press, Washington, D.C., 2011); and the National
661 Institutes of Health, Office of Laboratory Animal Welfare. Whenever possible, procedures
662 in this study were designed to avoid or minimize discomfort, distress, and pain to animals.
663 Animals were observed for signs of morbidity and/or mortality at least once daily,
664 according to animal welfare act and the Association for Assessment and Accreditation of
665 Laboratory Animal Care International (AAALACi). All mouse procedures were approved
666 by the Labcorp Institutional Animal Care and Use Committee (IACUC).
667
668 7-8 week-old female BALB/c mice (Charles River Laboratories) were purchased and
669 housed at Labcorp Drug Development, Denver, PA for immunization studies. All animals
670 were healthy upon receipt and were weighed and monitored during a 7-day acclimation

671 period before the start of the study. Mice were randomly assigned to experimental cohorts
672 of 10 animals. Up to 10 mice were co-housed together, and cages were kept in a climate-
673 controlled room at 63 to 77ºC at 50±20% relative humidity. Mice were provided Rodent
674 Diet #5001 (Purina Lab Diet) ad libitum.
675
676 2 µg of Wu1 S mRNA-LNP were administered to all cohorts of mice by IM injections on
677 days 0 and 28. On day 230, pre-vaccinated mice received different boosters by IM
678 injection: i) 2 µg Wu1 S mRNA-LNP; ii) 2 µg Wu1 S-EABR mRNA-LNP; iii) 1 µg Wu1 S
679 mRNA-LNP + 1 µg BA.5 S mRNA-LNP; iv) 1 µg Wu1 S-EABR mRNA-LNP + 1 µg BA.5
680 S-EABR mRNA-LNP. For bivalent boosters (iii and iv), the Wu1 and BA.5 S or S-EABR
681 mRNA-LNP were mixed prior to the IM injections. Serum samples for ELISAs and
682 neutralization assays were obtained on indicated days by retro-orbital bleeding. One
683 small drop of either 0.5% proparacaine hydrochloride ophthalmic solution or 0.5%
684 tetracaine hydrochloride ophthalmic solution was applied in the eye of the mouse prior to
685 performing retro-orbital blood collection. Eyes were alternated for each blood collection.
686 Euthanasia was performed in accordance with American Veterinary Medical Association
687 (AVMA) guidelines for euthanasia. Mice were individually placed in a CO2 chamber and
688 rendered unconscious. Mice were verified as unconscious by lack of response when toe
689 was pinched. Unconscious mice were subjected to bilateral jugular vein severance for
690 terminal exsanguination. Mice were placed back in the CO2 chamber until death
691 occurred. A double thoracotomy was performed as a second confirmation of death.
692
693

694 **Protein expression and purification**

695 Soluble SARS-CoV-2 S trimers (Wu1/D614G, BA.5, BQ.1.1, XBB.1)[32], RBDs (Wu1, BA.5,
696 BQ.1.1, XBB.1), and a prefusion-stabilized S2 protein[65] were expressed as described[37,66].
697 Briefly, Avi/His-tagged S trimers and His-tagged RBD and S2 proteins were purified from
698 transiently-transfected Expi293F cells (Gibco) by nickel affinity chromatography (HisTrap,
699 Cytiva) and size-exclusion chromatography (SEC) (Superose 6 Increase 10/300,
700 Cytiva)[33,37,66]. Peak fractions corresponding to S, RBD, or S2 proteins were pooled,
701 concentrated, and stored at 4ºC. Biotinylated S trimers for ELISAs were generated by co-
702 transfection of Avi/His-tagged S constructs with a plasmid encoding an endoplasmic
703 reticulum-directed BirA enzyme (kind gift from Michael Anaya, Caltech).

704

705 For heterotrimeric constructs, Wu1/BA.1 (HT2) and Wu1/BA.1/Delta (HT3) heterotrimers
706 were expressed via the addition of C-terminal tags and co-transfection of Expi293F cells
707 (Gibco) with specific plasmid DNA ratios. HT2 heterotrimers were produced by co-
708 transfecting a 1:1 plasmid DNA ratio of StrepII-tagged Wu1 S and His-tagged BA.1 S
709 constructs. HT3 heterotrimers were produced by co-transfecting a 1:1:1 plasmid DNA
710 ratio of StrepII-tagged Wu1 S, His-tagged BA.1 S, and D7324[47]-tagged Delta S
711 constructs. HT2 was sequentially purified using StrepTrap (Cytiva), HisTrap (Cytiva), and
712 SEC, while HT3 also underwent immunoaffinity chromatography using the D7324-specific
713 monoclonal Ab JR-52[47] (kind gift from James Robinson, Tulane University) before SEC.

714

715 The Wu1-His/Wu1-StrepII S homotrimer was generated by co-transfecting Expi293F cells
716 with a 1:1 plasmid DNA ratio of His-tagged Wu1 S and StrepII-tagged Wu1 S, followed by

717 purification as described for the HT2 heterotrimer. Single-tagged S homotrimers included
718 StrepII-tagged Wu1 S, His-tagged BA.1 S, and D7324-tagged Delta S, each purified using
719 their respective affinity chromatography steps followed by SEC.
720

721 **Single-particle cryo-EM sample preparation**

722 Grids of SARS-CoV-2 S homotrimers and heterotrimers were prepared at a protein
723 concentration of 2 mg/mL. Prior to freezing, fluorinated octylmaltoside solution (Anatrace)
724 was added to the S proteins at a final concentration of 0.02%(w/v). Three µL of S proteins
725 were immediately applied to Quantifoil 300 mesh 1.2/1.3 grids (Electron Microscopy
726 Sciences) that were freshly glow discharged with the PELCO easiGLOW (Ted Pella) for
727 60 seconds at 20 mA. Grids were blotted for 3 seconds using Whatman No.1 filter paper
728 with 0 blot force, 100% humidity and room temperature, and vitrified in 100% liquid ethane
729 using a Vitrobot Mark IV system (Thermo Fisher Scientific).
730

731 **Single-particle cryo-EM data collection and processing**

732 Single-particle cryo-EM datasets for SARS-CoV-2 S homotrimers and heterotrimers were
733 collected using SerialEM automatic data collection software[67] on a 300 keV Titan Krios
734 (Thermo Fisher Scientific) cryo-electron microscope equipped with a K3 direct electron
735 detector camera (Gatan). Movies were acquired in 40 frames with a defocus range of -1
736 to -3 µm and a total dosage of 60 electrons per $Å^2$ using the 3 by 3 beam image shift
737 pattern with 3 exposures per hole in the super-resolution mode at a pixel size of 0.416 Å.
738 Data processing workflows are outlined in Figure S10. For all datasets, motion correction
739 was done with patch motion correction with a binning factor of 2 and contrast transfer

740 function (CTF) parameters were estimated with Patch CTF in cryoSPARC[68]. Particles with
741 a diameter of 100 to 200 Å were picked with blob picker, inspected, extracted, and finally
742 classified with 2D classification in cryoSPARC[68]. Ice particles, junk particles, and particles
743 with preferred orientations were discarded, and the remaining particles were used for *ab*
744 *initio* reconstruction of three to four volumes. These reconstructions were further refined
745 with heterogeneous refinement in cryoSPARC[68]. Depending on the state for the receptor-
746 binding domains (RBDs) in the reconstructions, particles were combined for
747 homogeneous and non-uniform refinements to obtain the final reconstructions in
748 cryoSPARC[68].
749
750 **ELISAs**
751 ELISAs were performed as described[31,44]. To analyze serum binding to S trimers, pre-
752 blocked streptavidin-coated Nunc® MaxiSorp™ 384-well plates (ThemoFisher Scientific)
753 were coated with 5 µg/mL biotinylated S trimers in TBS-T/3% BSA for 1 hour at room
754 temperature. To analyze serum binding to RBDs or S2, Nunc® MaxiSorp™ 384-well
755 plates (Sigma) were coated with 2.5 µg/mL RBD or S2 in 0.1 M $NaHCO_3$ pH 9.8 and
756 incubated overnight at 4°C. Plates were blocked with TBS-T/3% BSA for 1 hour at room
757 temperature followed by removal of the blocking buffer by aspiration. Serum samples from
758 immunized mice were diluted 1:100, 4-fold serially diluted in TBS-T/3% BSA, and added
759 to plates. After a 3-hour incubation at room temperature, plates were washed with TBS-
760 T using an automated plate washer. HRP-conjugated goat anti-mouse IgG (715-035-150;
761 Jackson ImmunoResearch) was diluted 1:100,000 in TBS-T/3% BSA and added to plates
762 for 1 hour at room temperature. After washing with TBS-T, plates were developed using

763 SuperSignal™ ELISA Femto Maximal Signal Substrate (Thermo Fisher Scientific) and
764 absorbance was measured at 425 nm. Area under the curve (AUC) calculations for
765 binding curves were performed using GraphPad Prism 9.3.1 assuming a one-site binding
766 model with a Hill coefficient as described[69].
767
768 **Neutralization assays**
769 Lentivirus-based SARS-CoV-2 pseudoviruses were generated as described[35,36] using S
770 proteins from the Wu1/D614G, BA.1, BA.5, BQ.1.1, and XBB.1 variants in which the C-
771 terminal 21 residues of the S cytoplasmic tails were removed[35]. Serum samples from
772 immunized mice were heat-inactivated for 30 min at 56ºC. Three-fold serial dilutions of
773 heat-inactivated samples were incubated with pseudoviruses for 1 hour at 37ºC, followed
774 by addition of the serum-virus mixtures to pre-seeded HEK293T-ACE2 target cells. After
775 48-hour incubation at 37ºC, BriteLite Plus substrate (Perkin Elmer) was added and
776 luminescence was measured. Half-maximal inhibitory dilutions (ID_{50}s) were calculated
777 using 4-parameter non-linear regression analysis in AntibodyDatabase[70] and ID_{50} values
778 were rounded to three significant figures.
779
780 **Ab depletions**
781 HiTrap™ NHS-activated resin (Cytiva) was coupled to purified SARS-CoV-2 Wu1 RBD or
782 a mock protein (HIV-1 gp120) at a 10 mg/mL concentration and stored in PBS
783 supplemented with 0.02% sodium azide at 4°C. For Ab depletions, 50 µL dry worth of
784 RBD-coupled resin were aliquoted into microcentrifuge tubes and spun down at 13,000 x
785 g for 2 minutes. The supernatant was discarded. The resin was washed with 100 µL of

786 sterile PBS to remove excess PBS-azide solution. The supernatant was again discarded.
787 10 µL of mouse serum was then diluted in 90 µL PBS, and added to the resin. The tubes
788 were mixed and incubated at room temperature for 10 minutes. The resin-serum mixture
789 was spun down at 13,000 x g for 7 minutes to allow the resin to settle, and 90 µL of the
790 supernatant was transferred into a fresh microcentrifuge tube. To ensure no resin was
791 present in the final sample, the collection tube was spun down again, and supernatant
792 was transferred to a fresh microcentrifuge tube. Sterile PBS was added for a final volume
793 of 200 µL. Prior to neutralization assays, the Ab depleted serum samples were heat-
794 inactivated at 56°C for 30 minutes.
795
796 **Deep mutational scanning**
797 DMS studies to map RBD epitopes recognized by serum Abs were performed in biological
798 duplicates using independent mutant RBD yeast libraries (Wu1[42,71] and XBB.1.5 RBD[43]
799 libraries were generously provided by Tyler Starr, University of Utah) as
800 described[44,66,72,73]. Briefly, yeast libraries were stained with serum Abs, labeled with a
801 secondary Ab (115-605-008, Jackson ImmunoResearch), and then processed using a
802 Sony SH800 cell sorter. Cells were gated to capture RBD mutants that had reduced Ab
803 binding for a relatively high degree of RBD expression. Ab-escaped cells were expanded
804 for DNA extraction and Illumina sequencing was done as described[44,72,73]. Raw
805 sequencing data are available on the NCBI SRA under BioProject PRJNA1067836.
806 Escape fractions were computed using previously described processing steps[44,72,73] and
807 implemented using a Swift DMS program available from authors upon request.
808

809 Escape map visualizations shown as static line plots, logo plots and structural depictions
810 were all created using Swift DMS as previously described[41,44,73]. In some visualizations,
811 RBD sites were categorized based on epitope region, which were defined as class 1 (pink)
812 (RBD residues 403, 405, 406, 417, 420, 421, 453, 455-460, 473-478, 486, 487, 489, 503,
813 504), class 2 (purple) (residues 472, 479, 483-485, 490-495), class 3 (blue) (residues
814 341, 345, 346, 437-450, 496, 498-501), class 4 (orange) (residues 365-390, 408)[74], or
815 class 5 (green) (352-357, 396, 462-468)[41]. Structural visualizations were performed using
816 an RBD surface (PDB 6M0J) colored by the site-wise escape metric at each site as
817 described[44].
818
819 **Statistical analysis**
820 Statistically significant titer differences between immunized cohorts of BALB/c mice (10
821 mice per cohort) for ELISAs were determined using analysis of variance (ANOVA) test
822 followed by Tukey's multiple comparison post hoc test calculated using Graphpad Prism
823 9.3.1. Titer differences between immunized cohorts of BALB/c mice for Wu1, BA.5,
824 BQ.1.1, and XBB.1 neutralization assays were determined using the non-parametric
825 Kruskal-Wallis test followed by Dunn's multiple comparison post hoc test calculated using
826 Graphpad Prism 9.3.1. For BA.1 neutralization titers, statistically significant differences
827 were determined using the non-parametric two-tailed Mann-Whitney test calculated using
828 Graphpad Prism 9.3.1.
829

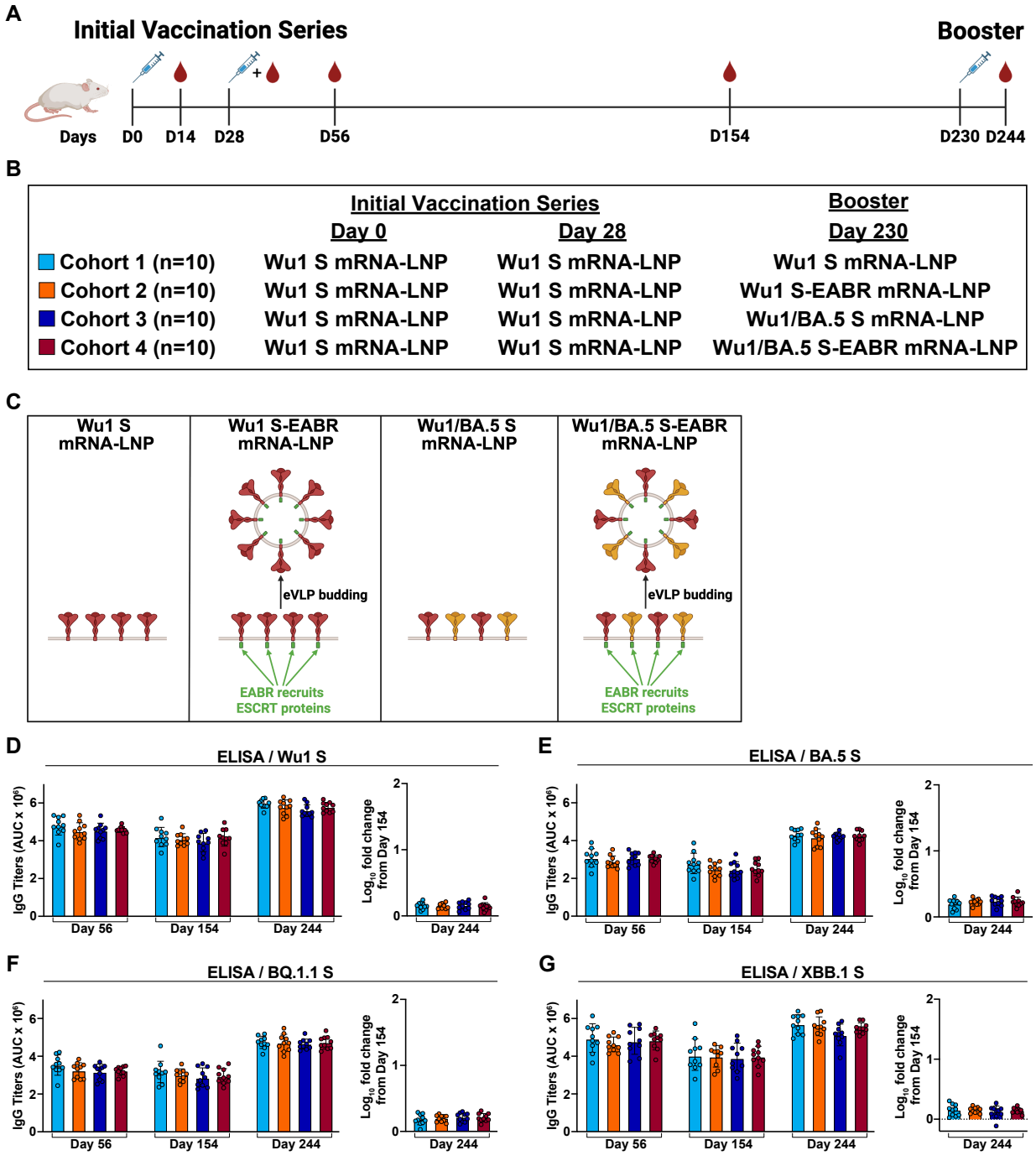

Figure 1. Monovalent and bivalent boosters elicit similar Ab binding responses against variant S trimers in pre-vaccinated mice. A) Immunization schedule in BALB/c mice. Blood samples were collected on days 14, 56, 154, and 244. This panel was created using BioRender.com. **B)** Immunization regimens for each cohort. All cohorts were initially

835 vaccinated with 2 µg of Wu1 S mRNA-LNP on days 0 and 28 by IM injection. Pre-
836 vaccinated mice received different boost immunogens on day 230 by IM injection. Cohorts
837 1-4 received 2 µg of monovalent Wu1 S mRNA-LNP (cyan), monovalent Wu1 S-EABR
838 mRNA-LNP (orange), bivalent Wu1/BA.5 S mRNA-LNP (blue), or bivalent Wu1/BA.5 S-
839 EABR mRNA-LNP (maroon), respectively. **C)** Schematic showing the different boost
840 immunogens that were administered on day 230. Wu1 S mRNA-LNP immunization results
841 in cell surface presentation of membrane-anchored Wu1 S trimers. Wu1 S-EABR mRNA-
842 LNP immunization results in dual presentation of Wu1 S trimers on cell surfaces and on
843 eVLPs that are secreted after budding from the plasma membrane. eVLP formation is
844 induced by EABR-mediated recruitment of host cell proteins from the ESCRT pathway.
845 Bivalent Wu1/BA.5 S mRNA-LNP immunization results in cell surface presentation of
846 membrane-anchored Wu1 and BA.5 S trimers. Wu1/BA.5 S-EABR mRNA-LNP
847 immunization results in dual presentation of Wu1 and BA.5 S trimers on cell surfaces and
848 eVLPs that bud from the plasma membrane. S trimers are shown as homotrimers for both
849 monovalent and bivalent boost immunogens. This panel was created
850 using BioRender.com. **D-G)** ELISA data from indicated time points for antisera from
851 individual mice (colored circles) presented as the geometric mean (bars) and standard
852 deviation (horizontal lines) of area under the curve (AUC) values. ELISAs evaluated
853 binding of purified Ss from the **D)** Wu1, **E)** BA.5, **F)** BQ.1.1, and **G)** XBB.1 variants. The
854 $\log_{10}$-fold change in binding titers from day 154 to day 244 is also shown for each S
855 (plotted as mean (bars) and standard deviation (horizontal lines)).
856

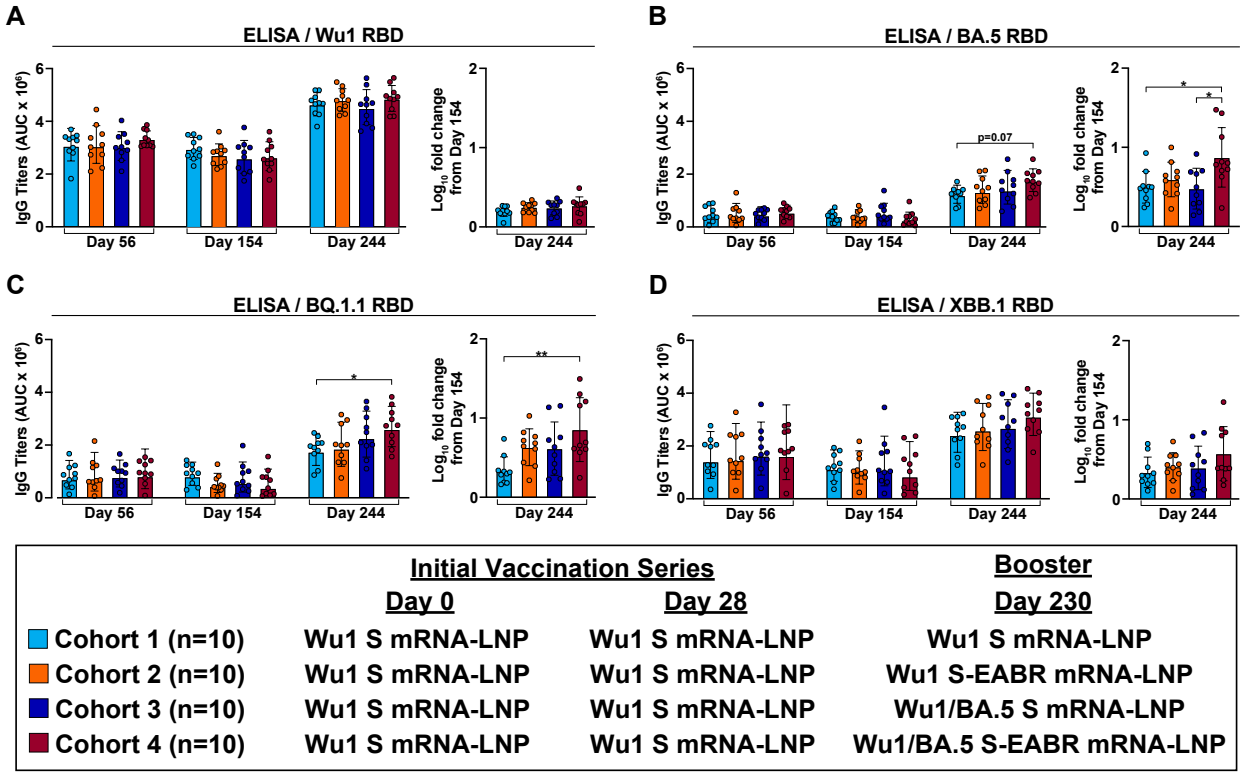

	Initial Vaccination Series		Booster
	Day 0	Day 28	Day 230
Cohort 1 (n=10)	Wu1 S mRNA-LNP	Wu1 S mRNA-LNP	Wu1 S mRNA-LNP
Cohort 2 (n=10)	Wu1 S mRNA-LNP	Wu1 S mRNA-LNP	Wu1 S-EABR mRNA-LNP
Cohort 3 (n=10)	Wu1 S mRNA-LNP	Wu1 S mRNA-LNP	Wu1/BA.5 S mRNA-LNP
Cohort 4 (n=10)	Wu1 S mRNA-LNP	Wu1 S mRNA-LNP	Wu1/BA.5 S-EABR mRNA-LNP

Figure 2. Bivalent S-EABR mRNA-LNP booster elicits potent Ab responses targeting Omicron RBDs. A-D) RBD binding titers for antisera from pre-vaccinated mice that received booster immunizations with 2 µg of monovalent Wu1 S mRNA-LNP (cyan), 2 µg of monovalent Wu1 S-EABR mRNA-LNP (orange), 2 µg of bivalent Wu1/BA.5 S mRNA-LNP (blue), or 2 µg of bivalent Wu1/BA.5 S-EABR mRNA-LNP (maroon) (immunization schedule in Fig. 1A-B). ELISA data are shown for indicated time points for antisera from individual mice (colored circles) presented as the geometric mean (bars) and standard deviation (horizontal lines) of area under the curve (AUC) values. ELISAs evaluated binding of RBDs from the **A)** Wu1, **B)** BA.5, **C)** BQ.1.1, and **D)** XBB.1 SARS-CoV-2 variants. The $\log_{10}$-fold change in binding titers from day 154 to day 244 is also shown for each RBD (plotted as mean (bars) and standard deviation (horizontal lines)).

869 Significant differences between cohorts linked by horizontal lines are indicated by

870 asterisks: $p<0.05$ = *, $p<0.01$ = **.

871

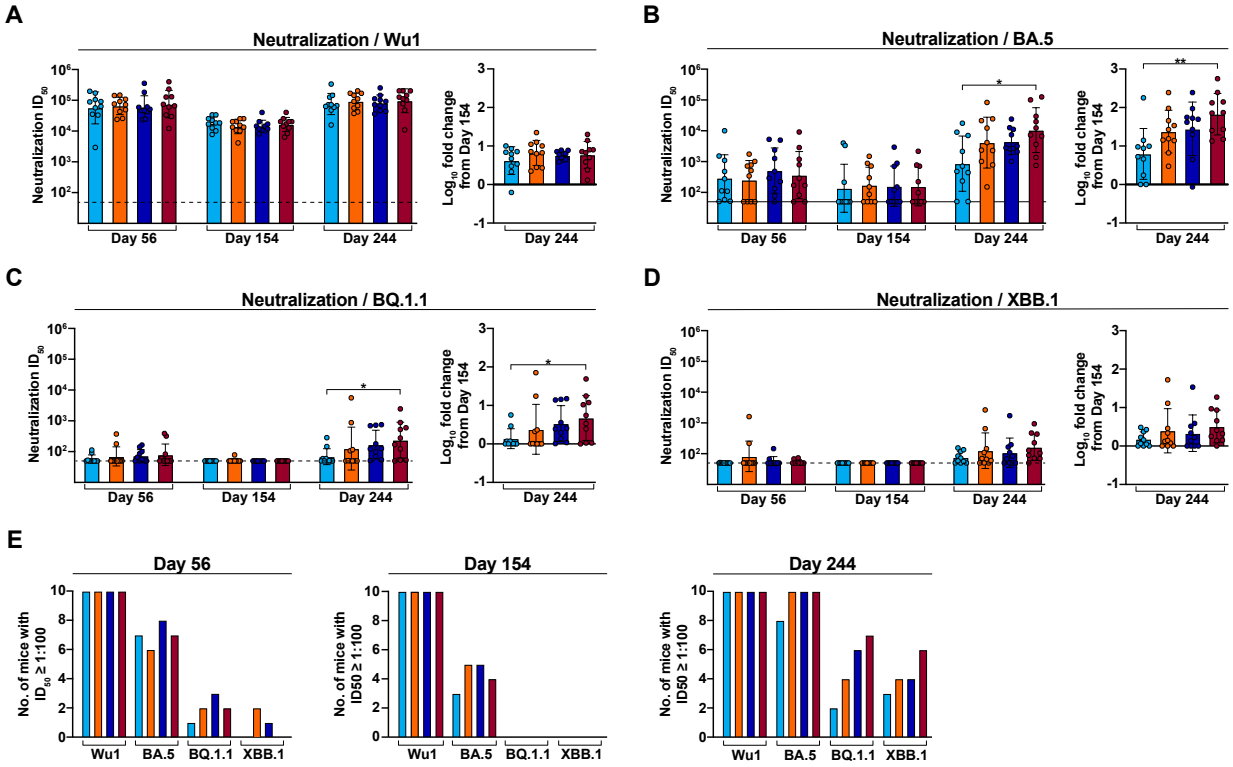

	Initial Vaccination Series		Booster
	Day 0	Day 28	Day 230
Cohort 1 (n=10)	Wu1 S mRNA-LNP	Wu1 S mRNA-LNP	Wu1 S mRNA-LNP
Cohort 2 (n=10)	Wu1 S mRNA-LNP	Wu1 S mRNA-LNP	Wu1 S-EABR mRNA-LNP
Cohort 3 (n=10)	Wu1 S mRNA-LNP	Wu1 S mRNA-LNP	Wu1/BA.5 S mRNA-LNP
Cohort 4 (n=10)	Wu1 S mRNA-LNP	Wu1 S mRNA-LNP	Wu1/BA.5 S-EABR mRNA-LNP

Figure 3. Bivalent Wu1/BA.5 S-EABR mRNA-LNP booster elicits higher neutralizing responses against Omicron subvariants. A-D) Neutralization titers for antisera from pre-vaccinated mice that received booster immunizations with 2 µg of monovalent Wu1 S mRNA-LNP (cyan), 2 µg of monovalent Wu1 S-EABR mRNA-LNP (orange), 2 µg of bivalent Wu1/BA.5 S mRNA-LNP (blue), or 2 µg of bivalent Wu1/BA.5 S-EABR mRNA-LNP (maroon) (immunization schedule in Fig. 1A-B). Neutralization data are shown for indicated time points for antisera from individual mice (colored circles) presented as the geometric mean (bars) and standard deviation (horizontal lines) of ID_{50} values. Results are shown for **A)** Wu1, **B)** BA.5, **C)** BQ.1.1, and **D)** XBB.1 pseudoviruses. Dashed

882 horizontal lines correspond to the background values representing the limit of detection
883 for neutralization assays (ID_{50} = 1:50). The log_{10}-fold change in neutralization titers from
884 day 154 to day 244 is also shown for each pseudovirus (plotted as mean (bars) and
885 standard deviation (horizontal lines)). Significant differences between cohorts linked by
886 horizontal lines are indicated by asterisks: $p<0.05$ = *, $p<0.01$ = **. **E)** Number of mice in
887 each cohort that reached an $ID_{50} \leq$ 1:100 against each variant on days 56 (left), 154
888 (middle), and 244 (right).
889

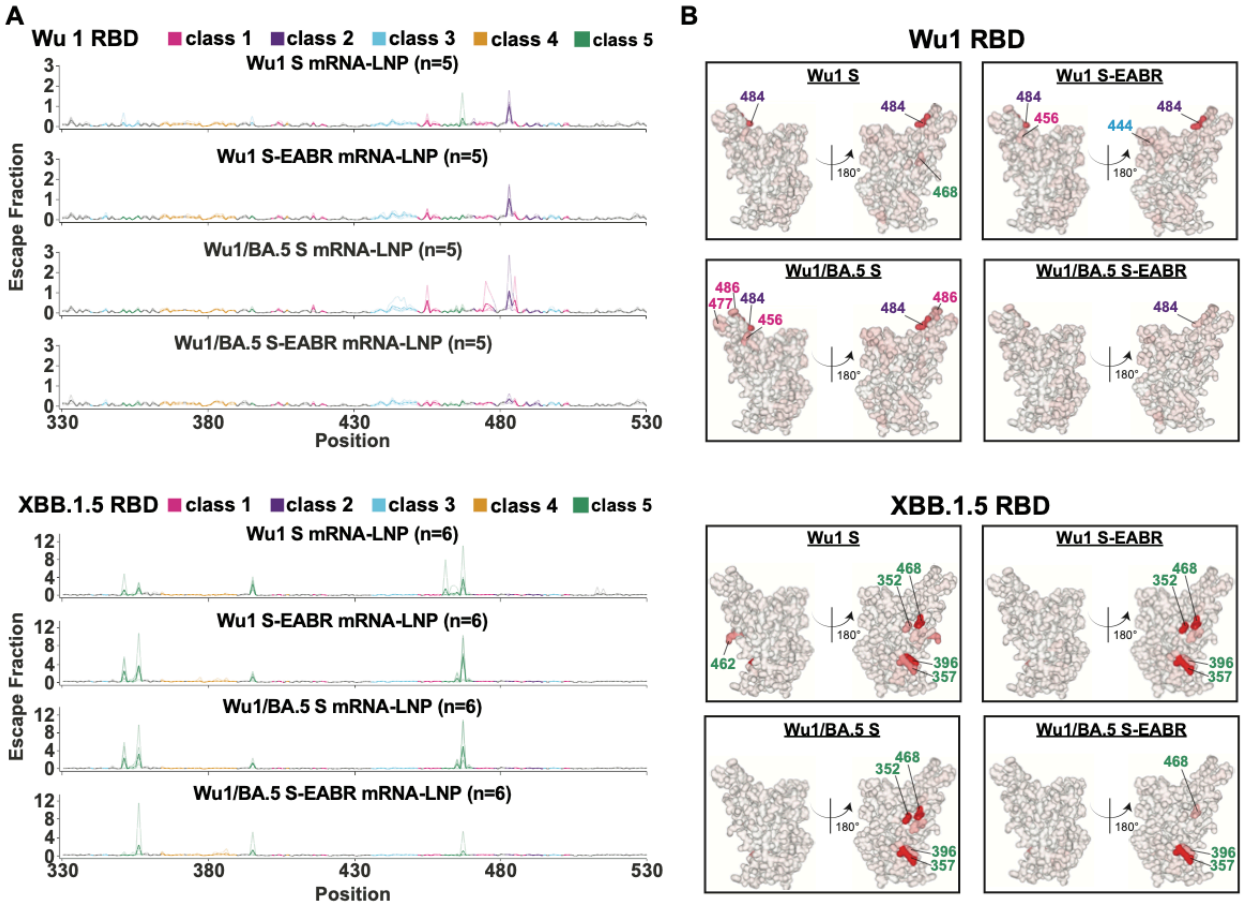

Figure 4. Bivalent S-EABR mRNA-LNP booster induces polyclass Ab responses. Sera for DMS studies were derived from pre-vaccinated mice that received booster immunizations with 2 µg of monovalent Wu1 S mRNA-LNP, monovalent Wu1 S-EABR mRNA-LNP, bivalent Wu1/BA.5 S mRNA-LNP, or bivalent Wu1/BA.5 S-EABR mRNA-LNP (immunization schedule in Fig. 1A-B). DMS was performed for 6 serum samples for each cohort, which were selected based on XBB.1 neutralization activity (1st, 2nd, 3rd, 5th, 6th, and 10th best neutralizer from each cohort). For the Wu1 RBD library, only five DMS profiles were obtained for each cohort. **A)** Line plots for DMS results using Wu1 (top) or XBB.1.5 (bottom) RBD libraries for sera from pre-vaccinated mice that received the indicated boost immunogens. The x axes display the RBD residue numbers, and the y

901 axes show the sum of the Ab escape of all mutations at a site (larger numbers indicating
902 increased Ab escape). Each faint line shows one antiserum with heavy lines representing
903 the average across the n = 5 (top) or n = 6 (bottom) sera in each cohort. Lines are colored
904 differently for RBD epitopes within different RBD epitope classes[33,40] (color definitions
905 shown in legend above line plots; epitopes are shown in Fig. S2; gray color for residues
906 not assigned to an epitope). **B)** The average site-total Ab escape for the Wu1 (top) or
907 XBB.1.5 (bottom) RBD libraries for pre-vaccinated mice that received the indicated boost
908 immunogens mapped to the Wu1 RBD surface (PDB: 6M0J). Gray coloring indicates no
909 escape, and red coloring indicates escape. Lines with numbers colored according to
910 epitope class indicate RBD positions with the most escape.

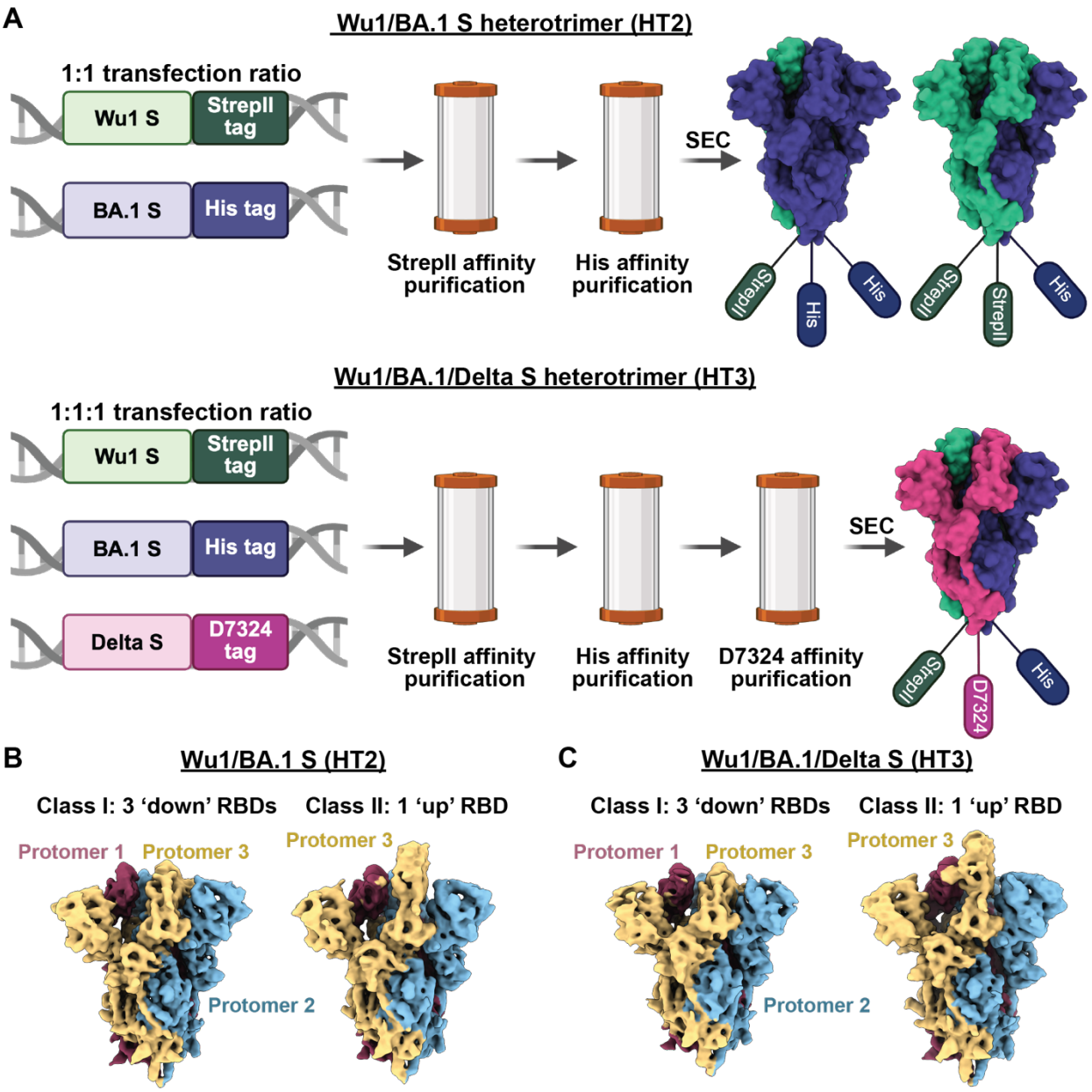

D

Trimers/ Heterotrimers \ Conformational states	0 'up' RBD 3 'down' RBDs	1 'up' RBD 2 'down' RBDs
Wu1/BA.1 S (HT2)	✔	✔
Wu1/BA.1/Delta S (HT3)	✔	✔
Wu1 S Tag Control (StrepII/His)	✔	✔
Wu1 S	✔	✔
BA.1 S	✔	✔
Delta S	✔	✔

911

912 **Figure 5. Heterotrimer S formation occurs for soluble constructs. A)** Schematic for
913 the generation and purification of soluble SARS-CoV-2 Wu1/BA.1 (HT2) and
914 Wu1/BA.1/Delta (HT3) S heterotrimers. HT2 heterotrimers were generated by co-
915 transfection of StrepII-tagged Wu1 S and His-tagged BA.1 S constructs at a 1:1 DNA
916 ratio, while HT3 heterotrimers were produced by co-transfecting StrepII-tagged Wu1 S,
917 His-tagged BA.1 S, and D7324-tagged Delta S constructs at a 1:1:1 ratio. Each
918 heterotrimer was sequentially purified using affinity chromatography specific for each tag
919 (StrepII, His, or JR-52) to ensure incorporation of distinct protomers. This panel was
920 created using BioRender.com. **B)** Cryo-EM density maps for Wu1/BA.1 HT2 S class I with
921 3 'down' RBDs (3.8 Å resolution) and class II with 1 'up' RBD (3.8 Å resolution). **C)** 4.0 Å
922 and 3.9 Å resolution cryo-EM density maps for Wu1/BA.1/Delta HT3 S with 3 'down' RBDs
923 and 1 'up' RBD. **D)** Table summarizing S heterotrimer and control homotrimer
924 conformational states.
925

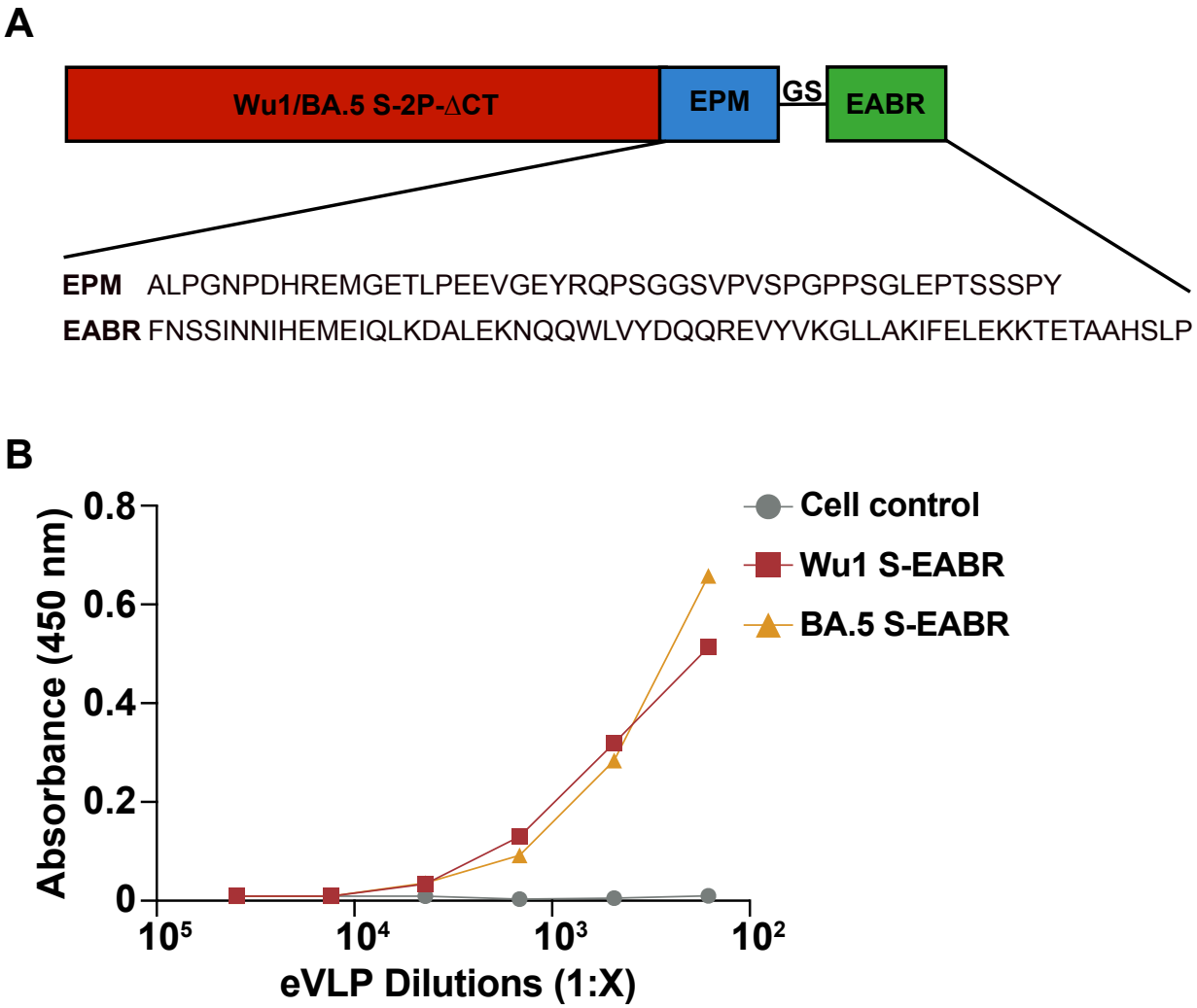

Figure S1. Wu1 and BA.5 S-EABR constructs induce efficient eVLP budding. A) Design and sequence information for SARS-CoV-2 S-EABR constructs. Top: The Wu1 and BA.5 S (including a furin cleavage site, 2P stabilizing substitutions, the D614G substitution, and ΔCT, a cytoplasmic tail deletion) were fused to an EPM sequence, a $(Gly)_3Ser$ (GS) spacer, and an EABR sequence. EPM = Endocytosis prevention motif. GS = $(Gly)_3Ser$ linker. EABR = ESCRT- and ALIX-binding region. Bottom: EPM and EABR sequence information. **B)** DNA plasmids encoding Wu1 S-EABR (red) or BA.5 S-EABR (orange) constructs were transfected into HEK293T cells. 48 hours post-transfection, transfected cell culture supernatants were harvested, and eVLPs were purified by

936 ultracentrifugation on a 20% sucrose cushion. Purified eVLP samples were serially
937 diluted, directly coated onto 96-well plates, and eVLP-associated S protein levels were
938 quantified by ELISA.
939

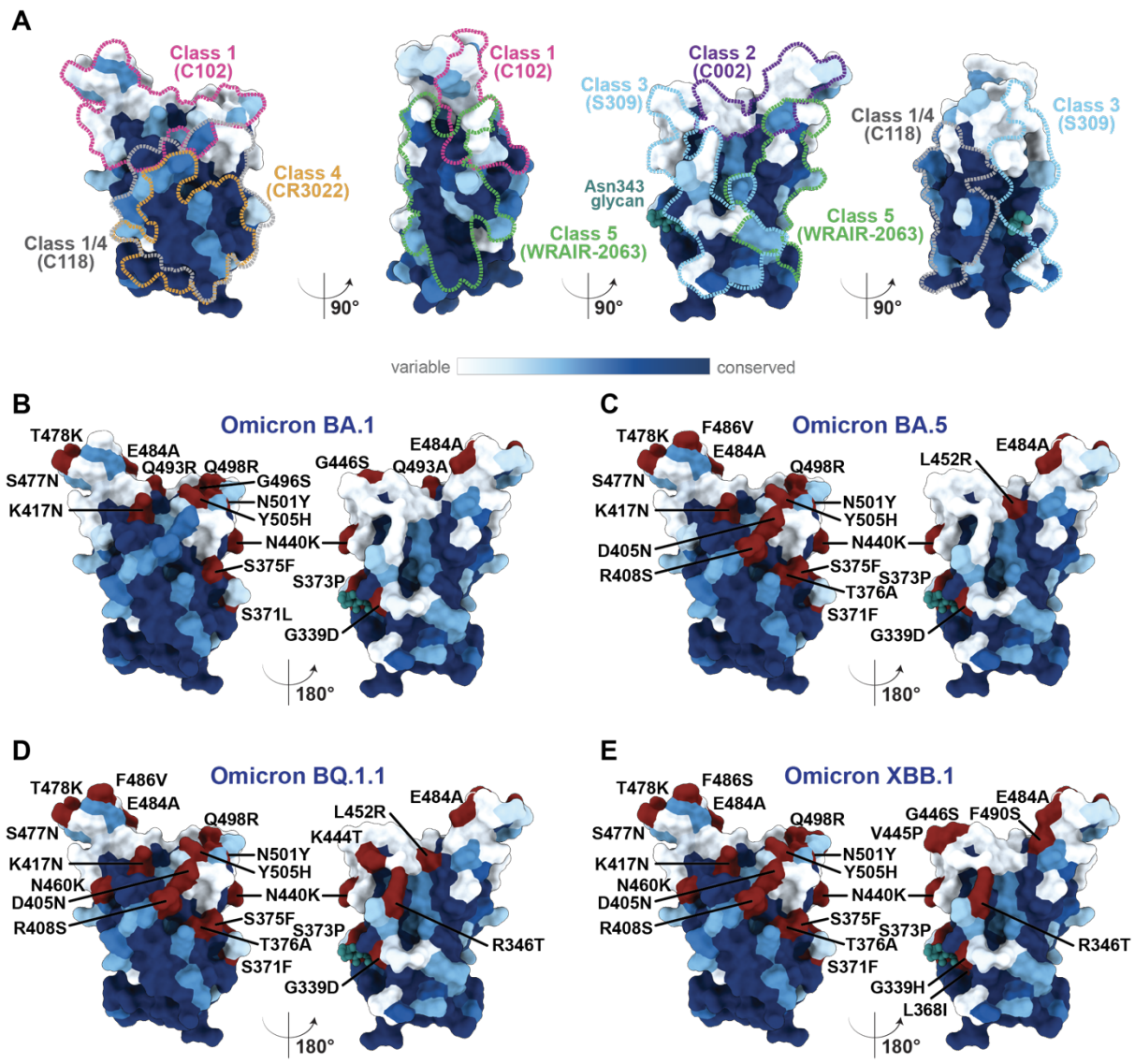

Figure S2. Sarbecovirus RBD sequence conservation. A) Sequence conservation of 16 sarbecovirus RBDs calculated with ConSurf[75] and plotted on a surface representation of a SARS-CoV-2 RBD (PDB 7BZ5). Anti-RBD class 1, 2, 3, 4, 1/4, and 5 Ab epitopes are outlined with dotted lines in different colors using structural information from representative structures of mAb bound to SARS-CoV-2 S or RBD (C102: PDB 7K8M; C002: PDB 7K8T, S309: PDB 7JX3; CR3022: PDB 7LOP; C118: PDB 7RKV; WRAIR-

947 2063: PDB 8EOO). SARS-CoV-2 RBD substitutions (colored in red) in Omicron **B)** BA.1,

948 **C)** BA.5, **D)** BQ.1.1, and **E)** XBB.1 variants plotted on the RBD sequence conservation

949 plot.

950

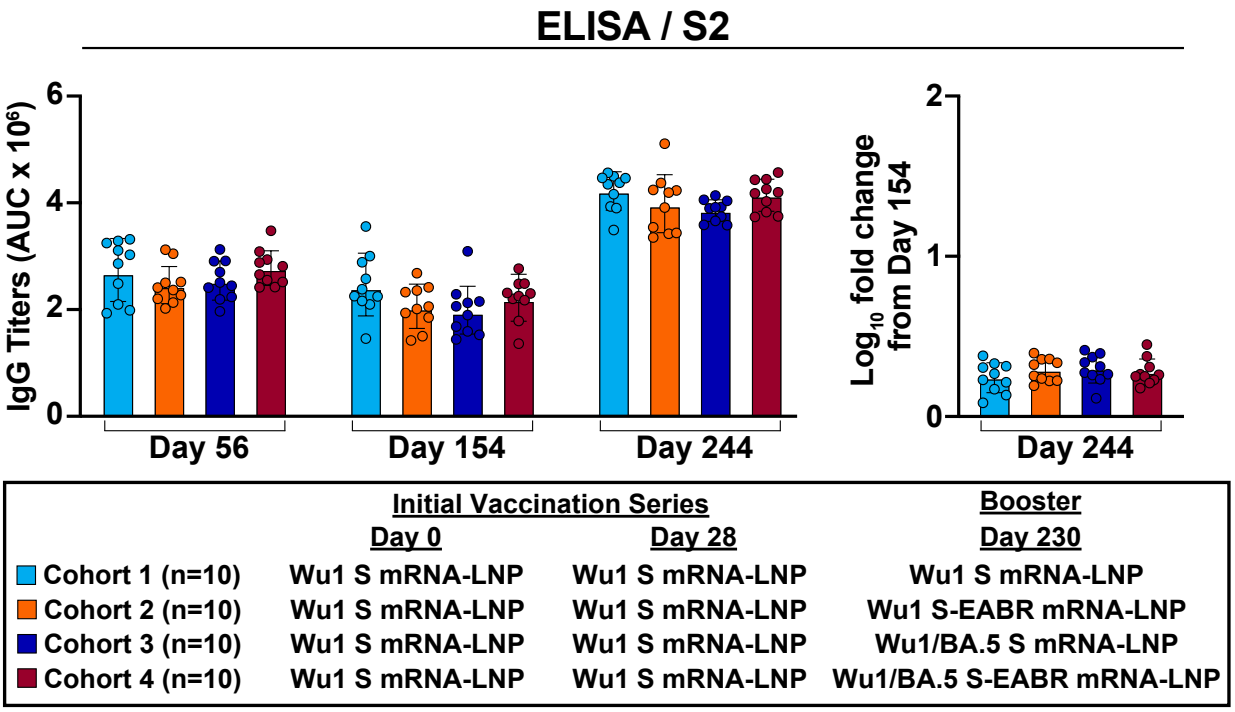

Figure S3. Primary vaccinations and booster immunizations elicit potent anti-S2 binding responses. S2 binding titers for antisera from pre-vaccinated mice that received booster immunizations with 2 µg of monovalent Wu1 S mRNA-LNP (cyan), 2 µg of monovalent Wu1 S-EABR mRNA-LNP (orange), 2 µg of bivalent Wu1/BA.5 S mRNA-LNP (blue), or 2 µg of bivalent Wu1/BA.5 S-EABR mRNA-LNP (maroon). ELISA data for binding of Wu1 S2 are shown for indicated time points for antisera from individual mice (colored circles) presented as the geometric mean (bars) and standard deviation (horizontal lines) of area under the curve (AUC) values. The $\log_{10}$-fold change in binding titers from day 154 to day 244 is also shown (plotted as mean (bars) and standard deviation (horizontal lines)).

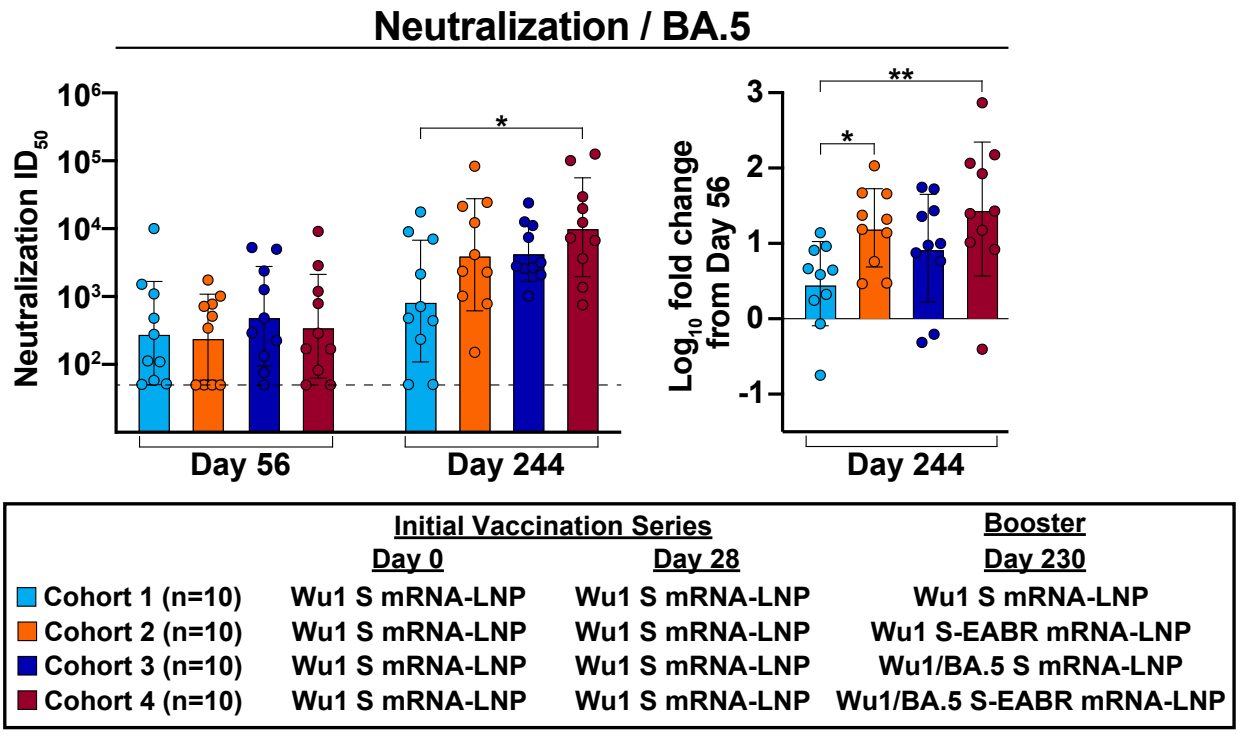

Figure S4. Monovalent and bivalent S-EABR mRNA-LNP boosters elicit higher increases in BA.5 neutralization compared to conventional S mRNA-LNP boosters. Neutralization titers for antisera from pre-vaccinated mice that received booster immunizations with 2 µg of monovalent Wu1 S mRNA-LNP (cyan), 2 µg of monovalent Wu1 S-EABR mRNA-LNP (orange), 2 µg of bivalent Wu1/BA.5 S mRNA-LNP (blue), or 2 µg of bivalent Wu1/BA.5 S-EABR mRNA-LNP (maroon) (immunization schedule in Fig. 1A-B). BA.5 neutralization data are shown for indicated time points for antisera from individual mice (colored circles) presented as the geometric mean (bars) and standard deviation (horizontal lines) of ID_{50} values. Dashed horizontal lines correspond to the background values representing the limit of detection for neutralization assays (ID_{50} = 1:50). The log_{10}-fold change in neutralization titers from day 56 to day 244 is also shown (plotted as mean (bars) and standard deviation (horizontal lines)). Significant differences

976 between cohorts linked by horizontal lines are indicated by asterisks: $p<0.05$ = *, $p<0.01$

977 = **.

978

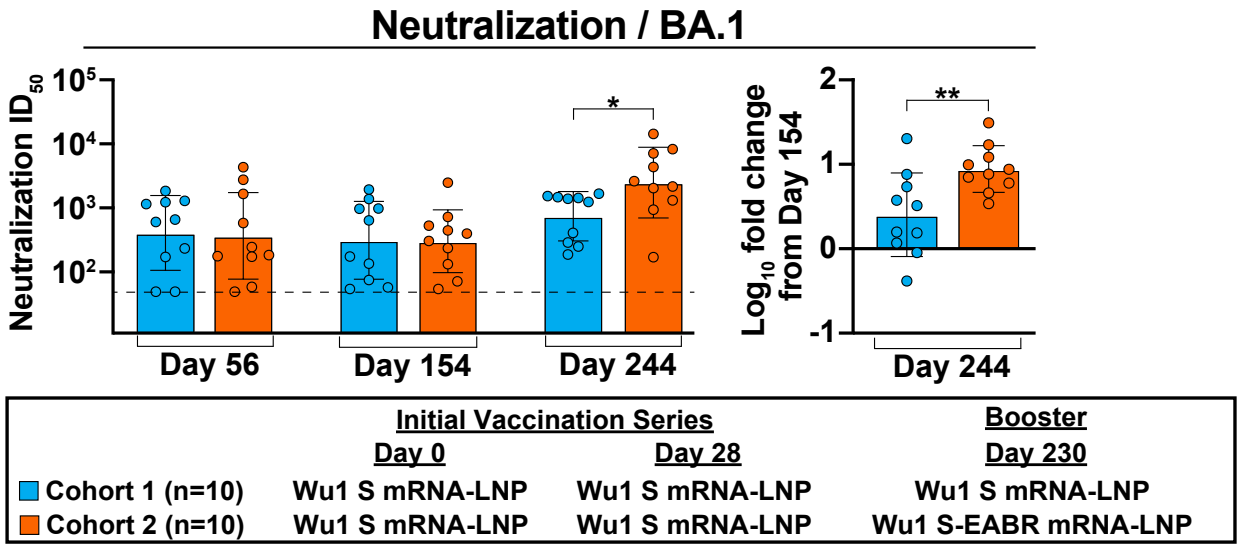

Figure S5. Monovalent Wu1 S-EABR mRNA-LNP booster elicits improved neutralizing responses against BA.1 variant. Neutralization titers for antisera from pre-vaccinated mice that received booster immunizations with 2 µg of monovalent Wu1 S mRNA-LNP (cyan) or monovalent Wu1 S-EABR mRNA-LNP (orange). Neutralization data are shown for indicated time points for antisera from individual mice (colored circles) presented as the geometric mean (bars) and standard deviation (horizontal lines) of ID_{50} values against BA.1 pseudovirus. Dashed horizontal lines correspond to the limit of detection for neutralization assays (ID_{50} = 1:50). The log_{10}-fold change in neutralization titers from day 154 to day 244 is also shown (plotted as mean (bars) and standard deviation (horizontal lines)). Significant differences between cohorts linked by horizontal lines are indicated by asterisks: $p<0.05$ = *.

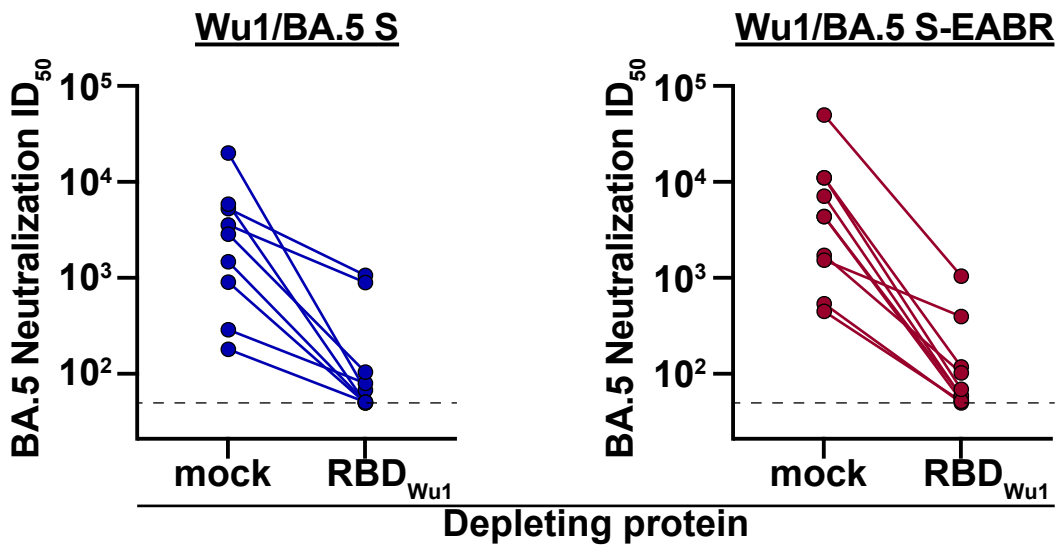

991

992 **Figure S6. Depleting bivalent booster-induced antisera with Wu1 RBD reduces**
993 **BA.5 neutralizing activity.** Day 244 serum samples obtained from pre-vaccinated mice
994 that received booster immunizations with 2 µg of bivalent Wu1/BA.5 S mRNA-LNP (blue)
995 or 2 µg of bivalent Wu1/BA.5 S-EABR mRNA-LNP (maroon) were depleted using a mock
996 protein (HIV-1 gp120; left) or Wu1 RBD (right). The neutralizing activity of the depleted
997 antisera was measured against BA.5 pseudovirus. Neutralization data are shown as ID_{50}
998 values for individual mice (colored circles). Data points for individual mice following mock
999 or Wu1 RBD depletions are connected by colored lines. Dashed horizontal lines
1000 correspond to the limit of detection for neutralization assays (ID_{50} = 1:50).

1001

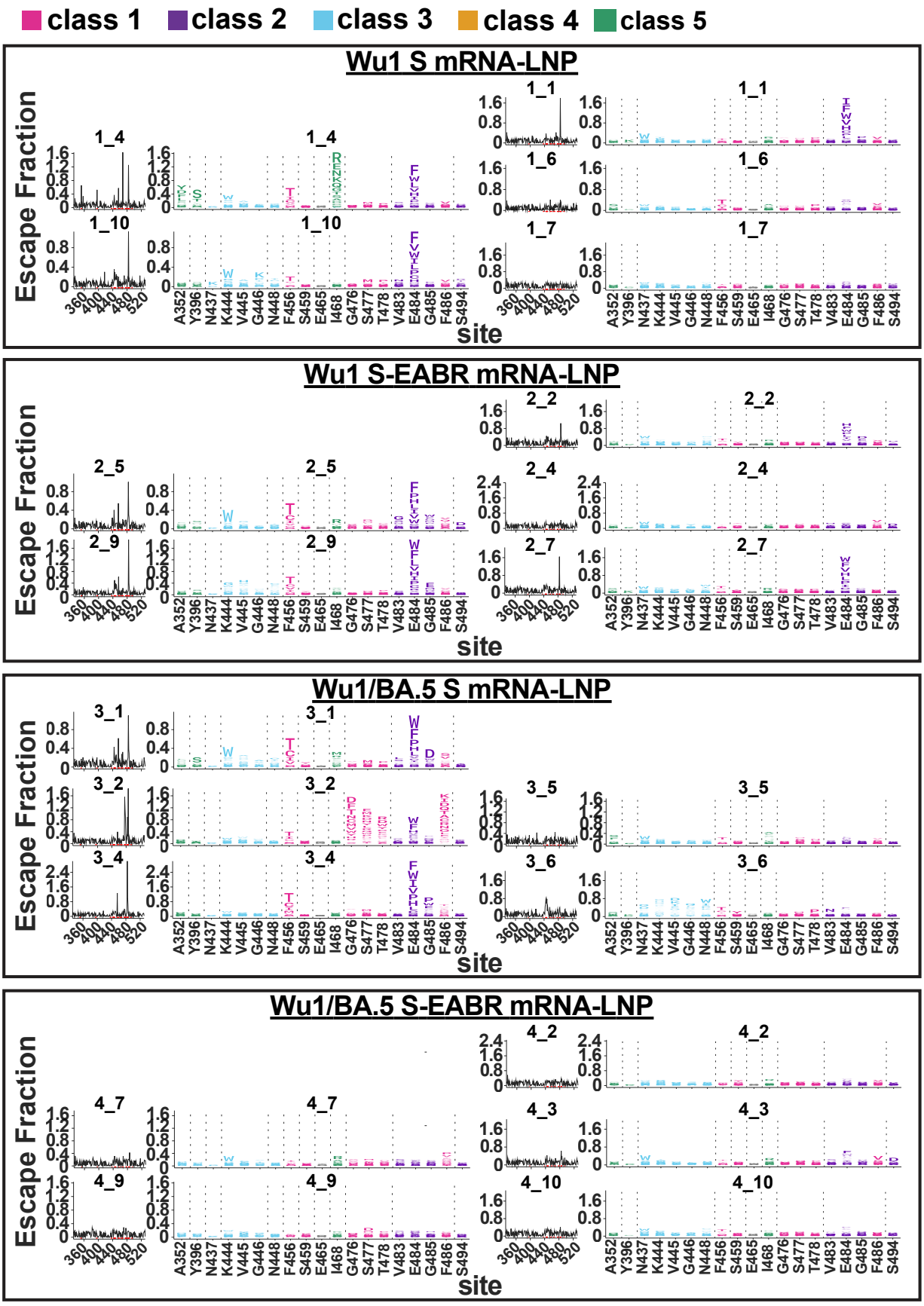
class 1
class 2
class 3
class 4
class 5
Wu1 S mRNA-LNP
Wu1 S-EABR mRNA-LNP
Wu1/BA.5 S mRNA-LNP
Wu1/BA.5 S-EABR mRNA-LNP
Escape Fraction
site
1_1
1_4
1_6
1_7
1_10
2_2
2_4
2_5
2_7
2_9
3_1
3_2
3_4
3_5
3_6
4_2
4_3
4_7
4_9
4_10
A352 Y396 N437 K444 V445 G446 N448 F456 S459 E465 I468 G476 S477 T478 V483 E484 G485 F486 S494

1002

1003 **Figure S7. Bivalent S-EABR mRNA-LNP booster induces polyclass Ab responses**
1004 **against Wu1 RBD.** Sera for DMS studies were derived from pre-vaccinated mice that
1005 received booster immunizations with 2 μg of monovalent Wu1 S mRNA-LNP, monovalent
1006 Wu1 S-EABR mRNA-LNP, bivalent Wu1/BA.5 S mRNA-LNP, or bivalent Wu1/BA.5 S-
1007 EABR mRNA-LNP (immunization schedule in Fig. 1A-B). Line (left) and logo plots (right)
1008 are shown for DMS results for individual sera from pre-vaccinated mice that received the
1009 indicated boost immunogens. DMS was performed using a Wu1 RBD library. The x axes
1010 of the line and logo plots display the RBD residue numbers. The y axis of the line plots
1011 shows the sum of the Ab escape of all mutations at a site (larger numbers indicating
1012 increased Ab escape). Sites with the strongest Ab escape are shown in logo plots, with
1013 tall letters representing the most frequent mutations at a site. Logo plots are colored
1014 differently for RBD epitopes within different classes[33,40,41] (epitopes are shown in Fig. S2;
1015 gray color for residues not assigned to an epitope).
1016

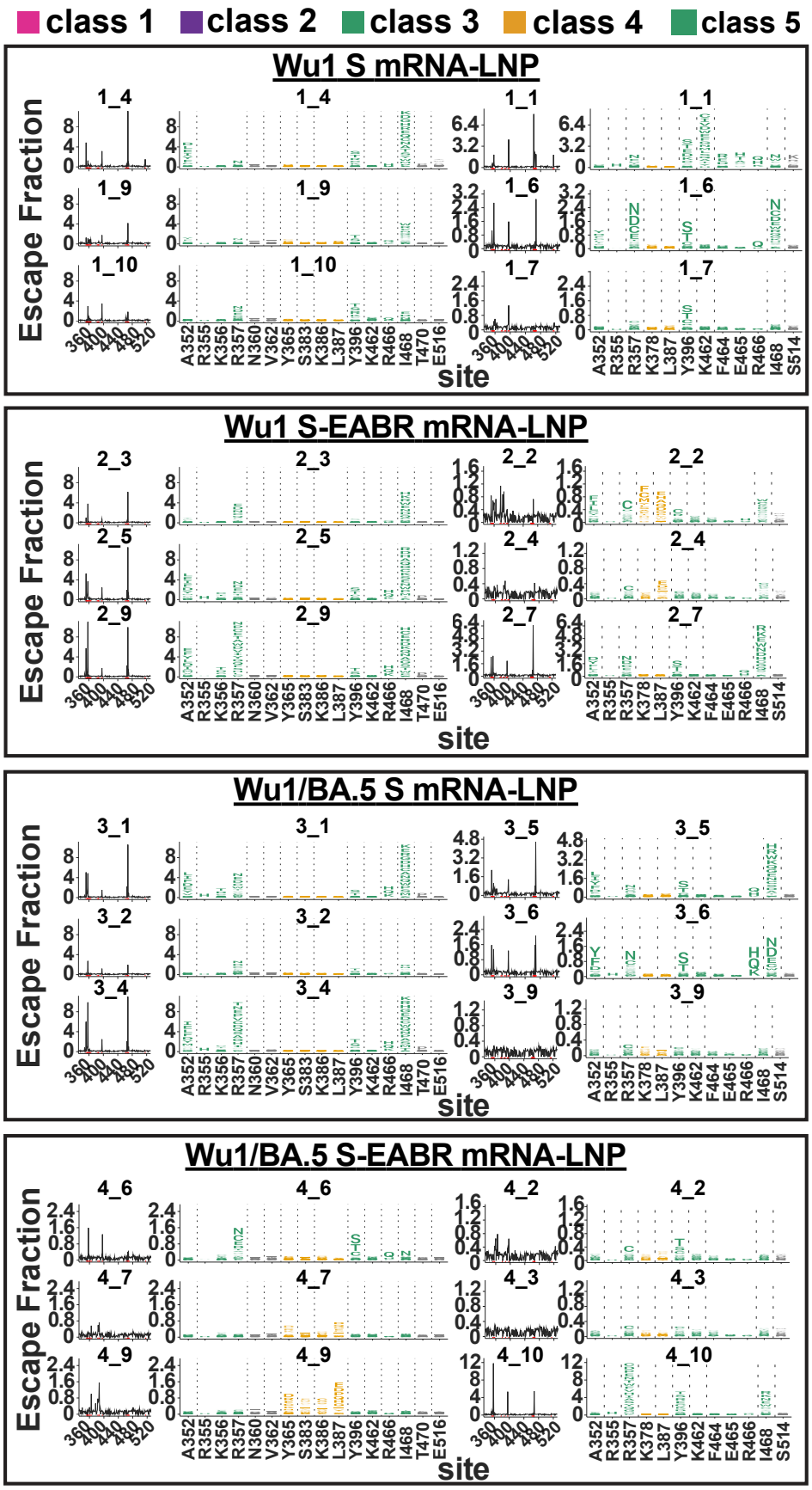
class 1
class 2
class 3
class 4
class 5
Wu1 S mRNA-LNP
Wu1 S-EABR mRNA-LNP
Wu1/BA.5 S mRNA-LNP
Wu1/BA.5 S-EABR mRNA-LNP
Escape Fraction
site

1017

1018 **Figure S8. Bivalent S-EABR mRNA-LNP booster induces less pronounced class 3**
1019 **Ab responses against XBB.1.5 RBD.** Sera for DMS studies were derived from pre-
1020 vaccinated mice that received booster immunizations with 2 μg of monovalent Wu1 S
1021 mRNA-LNP, monovalent Wu1 S-EABR mRNA-LNP, bivalent Wu1/BA.5 S mRNA-LNP, or
1022 bivalent Wu1/BA.5 S-EABR mRNA-LNP (immunization schedule in Fig. 1A-B). Line (left)
1023 and logo plots (right) are shown for DMS results for individual sera from pre-vaccinated
1024 mice that received the indicated boost immunogens. DMS was performed using an
1025 XBB.1.5 RBD library. The x axes of the line and logo plots display the RBD residue
1026 numbers. The y axis of the line plots shows the sum of the Ab escape of all mutations at
1027 a site (larger numbers indicating increased Ab escape). Sites with the strongest Ab
1028 escape are shown in logo plots, with tall letters representing the most frequent mutations
1029 at a site. Logo plots are colored differently for RBD epitopes within different
1030 classes[33,40] (epitopes are shown in Fig. S2; gray color for residues not assigned to an
1031 epitope).
1032

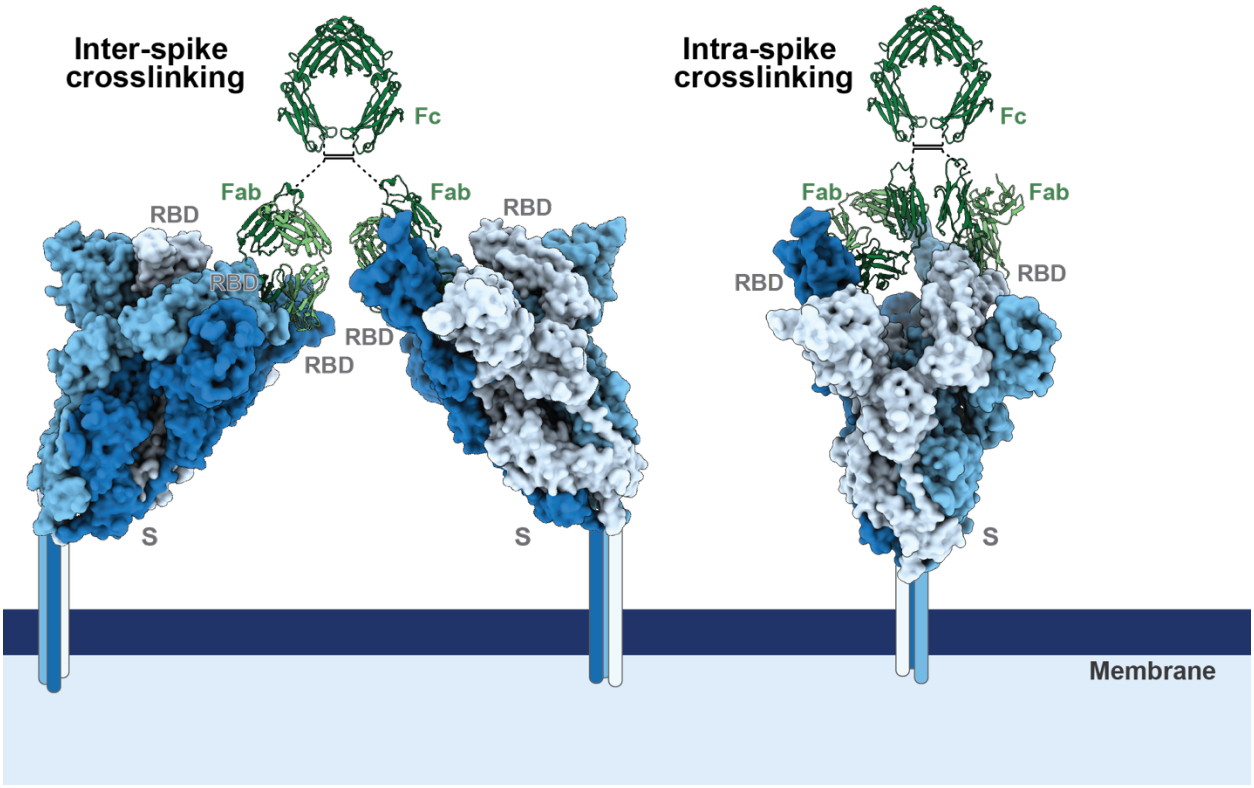

Figure S9. Cartoon diagram illustrating inter- and intra-S crosslinking. Left: model showing potential inter-S crosslinking through the interactions between both Fabs of a single IgG and two RBDs of adjacent viral S proteins. Right: model showing intra-S crosslinking through the interaction between both Fabs of a single IgG and two RBDs on the same viral S trimer. The hinge regions between the Fabs and Fc are modeled with flexible linkers, shown as dotted lines, as these regions were not resolved in the crystal structure of an intact IgG[76]. Disulfide bonds in the hinge region are shown as black lines. These diagrams are modeled based on the cryo-EM structure of SARS-CoV-2 S complexed with human C118 Fab (PDB ID 7RKV) and the crystal structure of human Fc (PDB ID 1FC1). IgGs shown in this figure represent either circulating Abs or membrane-bound BCRs.

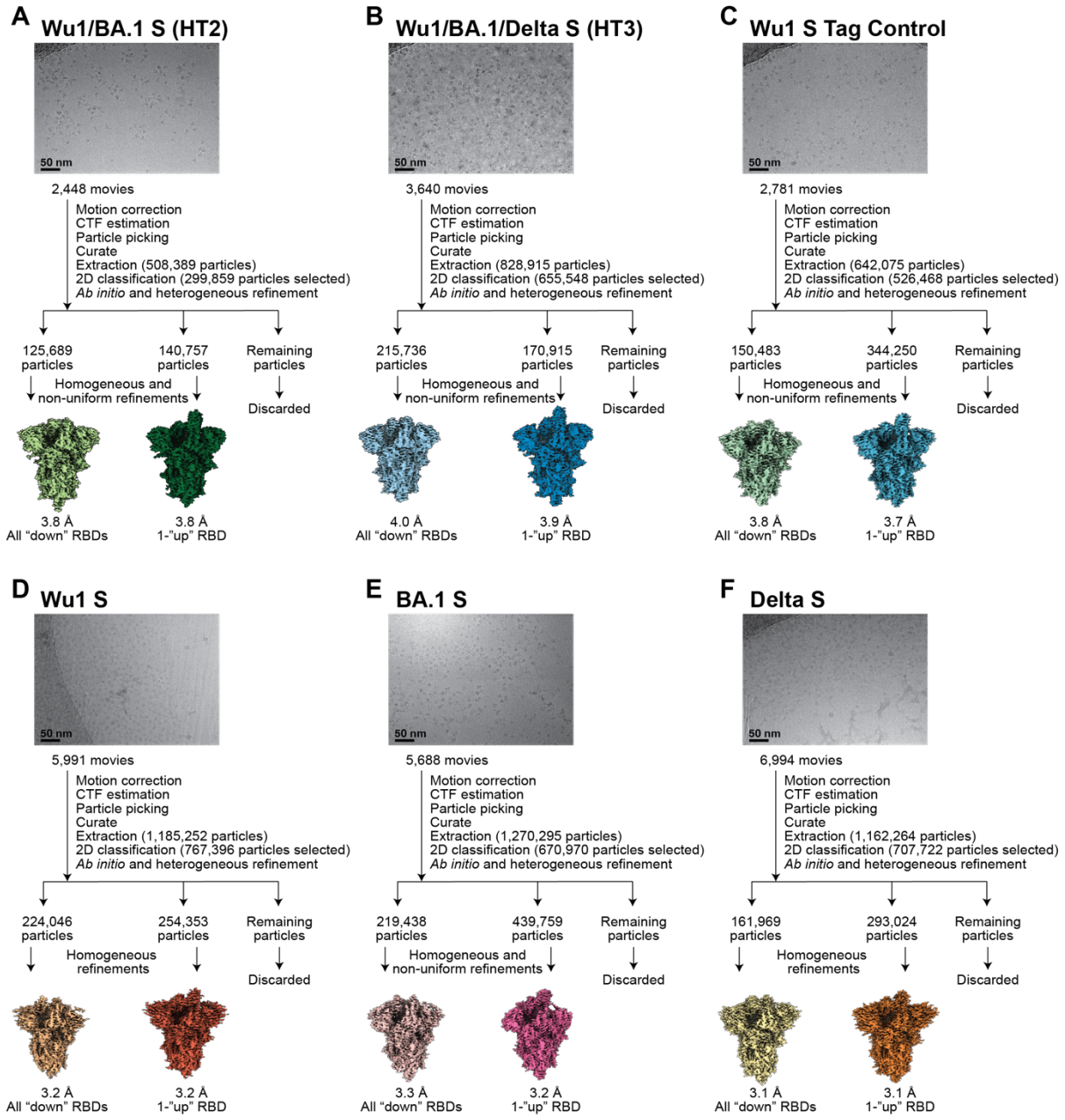

Figure S10. Cryo-EM data collection and processing for heterotrimeric and control SARS-CoV-2 S structures. Representative micrographs, workflow for single-particle data processing, and final reconstructions are shown for SARS-CoV-2 (**A**) Wu1/BA.1 S HT2 heterotrimer, (**B**) Wu1/BA.1/Delta S HT3 heterotrimer, and homotrimer S controls

1051 including (**C**) Wu1 His/StrepII double-tag control, (**D**) StrepII-tagged Wu1, (**E**) His-tagged

1052 BA.1, and (**F**) D7324-tagged Delta constructs.

1053

	Day 56				Day 154				Day 244			
	Wu1	**BA.5**	**BQ.1.1**	**XBB.1**	**Wu1**	**BA.5**	**BQ.1.1**	**XBB.1**	**Wu1**	**BA.5**	**BQ.1.1**	**XBB.1**
Cohort 1	56,855	274	58	50	17,843	136	50	50	74,875	851	69	75
Cohort 2	65,752	253	69	82	14,022	172	52	50	92,492	4,100	125	125
Cohort 3	60,300	513	74	57	14,130	159	50	50	80,978	4,441	169	108
Cohort 4	74,780	365	79	55	16,194	156	50	50	95,515	10,446	236	162

Table S1. Geometric mean neutralization titers. Day 56, 154, and 244 geometric mean neutralization titers for cohorts 1-4 against the Wu1, BA.5, BQ.1.1, and XBB.1 variants.

Boosting Immunogen	Animal	Wu1 DMS Profile	XBB.1.5 DMS Profile
Wu1 S mRNA-LNP	1_4	Moderate class 5 and 2	Strong class 5
Wu1 S mRNA-LNP	1_9		Strong class 5
Wu1 S mRNA-LNP	1_10	Moderate class 2	Strong class 5
Wu1 S mRNA-LNP	1_1	Moderate class 2	Strong class 5
Wu1 S mRNA-LNP	1_6	Polyclass	Strong class 5
Wu1 S mRNA-LNP	1_7	Polyclass	Moderate class 5
Wu1 S-EABR mRNA-LNP	2_3		Strong class 5
Wu1 S-EABR mRNA-LNP	2_5	Moderate class 2	Strong class 5
Wu1 S-EABR mRNA-LNP	2_9	Moderate class 2	Strong class 5
Wu1 S-EABR mRNA-LNP	2_2	Moderate class 2	Moderate class 5 and 4
Wu1 S-EABR mRNA-LNP	2_4	Polyclass	Polyclass
Wu1 S-EABR mRNA-LNP	2_7	Moderate class 2	Strong class 5
Wu1/BA.5 S mRNA-LNP	3_1	Moderate class 2	Strong class 5
Wu1/BA.5 S mRNA-LNP	3_2	Moderate class 1	Strong class 5
Wu1/BA.5 S mRNA-LNP	3_4	Strong class 2	Strong class 5
Wu1/BA.5 S mRNA-LNP	3_5	Polyclass	Strong class 5
Wu1/BA.5 S mRNA-LNP	3_6	Weak class 3	Strong class 5
Wu1/BA.5 S mRNA-LNP	3_9		Polyclass
Wu1/BA.5 S-EABR mRNA-LNP	4_6		Moderate class 5
Wu1/BA.5 S-EABR mRNA-LNP	4_7	Polyclass	Weak class 4
Wu1/BA.5 S-EABR mRNA-LNP	4_9	Polyclass	Moderate class 4
Wu1/BA.5 S-EABR mRNA-LNP	4_2	Polyclass	Weak class 5
Wu1/BA.5 S-EABR mRNA-LNP	4_3	Weak class 2	Polyclass
Wu1/BA.5 S-EABR mRNA-LNP	4_10	Polyclass	Strong class 5

	Escape fraction
Polyclass	<0.5
Weak	0.5-1
Moderate	1-2
Strong	>2

Table S2. Bivalent S-EABR mRNA-LNP booster induces consistent polyclass anti-RBD Ab responses. The DMS profiles for antisera from individual mice against the Wu1 and XBB.1.5 RBD libraries shown in Fig. S6 and S7 were classified as polyclass (total escape peaks <1 at all sites; green), moderate escape (total escape peaks between 1 and 2 at one or more sites; yellow), or strong escape (total escape peaks >2 at one or more sites; red) profiles. Total escape peaks represent the sum of escape fractions for all

1064 mutations at a specific site[45]. For moderate and strong escape profiles, the RBD epitope

1065 classes with the highest total escape peaks are specified.

References

1 Corbett, K. S. *et al.* SARS-CoV-2 mRNA vaccine design enabled by prototype pathogen preparedness. *Nature* **586**, 567-571 (2020). https://doi.org/10.1038/s41586-020-2622-0

2 Zheng, C. *et al.* Real-world effectiveness of COVID-19 vaccines: a literature review and meta-analysis. *Int J Infect Dis* **114**, 252-260 (2022). https://doi.org/10.1016/j.ijid.2021.11.009

3 Chen, Y. *et al.* Broadly neutralizing antibodies to SARS-CoV-2 and other human coronaviruses. *Nat Rev Immunol* **23**, 189-199 (2023). https://doi.org/10.1038/s41577-022-00784-3

4 Hogan, M. J. & Pardi, N. mRNA Vaccines in the COVID-19 Pandemic and Beyond. *Annu Rev Med* **73**, 17-39 (2022). https://doi.org/10.1146/annurev-med-042420-112725

5 Painter, M. M. *et al.* Rapid induction of antigen-specific CD4(+) T cells is associated with coordinated humoral and cellular immunity to SARS-CoV-2 mRNA vaccination. *Immunity* **54**, 2133-2142 e2133 (2021). https://doi.org/10.1016/j.immuni.2021.08.001

6 Oberhardt, V. *et al.* Rapid and stable mobilization of CD8(+) T cells by SARS-CoV-2 mRNA vaccine. *Nature* **597**, 268-273 (2021). https://doi.org/10.1038/s41586-021-03841-4

7 Polack, F. P. *et al.* Safety and Efficacy of the BNT162b2 mRNA Covid-19 Vaccine. *N Engl J Med* **383**, 2603-2615 (2020). https://doi.org/10.1056/NEJMoa2034577

8 Baden, L. R. *et al.* Efficacy and Safety of the mRNA-1273 SARS-CoV-2 Vaccine. *N Engl J Med* **384**, 403-416 (2021). https://doi.org/10.1056/NEJMoa2035389

9 Zhang, Z. *et al.* Humoral and cellular immune memory to four COVID-19 vaccines. *Cell* **185**, 2434-2451 e2417 (2022). https://doi.org/10.1016/j.cell.2022.05.022

10 Planas, D. *et al.* Reduced sensitivity of SARS-CoV-2 variant Delta to antibody neutralization. *Nature* **596**, 276-280 (2021). https://doi.org/10.1038/s41586-021-03777-9

11 Andrews, N. *et al.* Effectiveness of COVID-19 booster vaccines against COVID-19-related symptoms, hospitalization and death in England. *Nat Med* **28**, 831-837 (2022). https://doi.org/10.1038/s41591-022-01699-1

12 WHO. Classification of Omicron (B.1.1.529): SARS-CoV-2 variant of concern., (2021).

13 Liu, L. *et al.* Striking antibody evasion manifested by the Omicron variant of SARS-CoV-2. *Nature* **602**, 676-681 (2022). https://doi.org/10.1038/s41586-021-04388-0

14 Cele, S. *et al.* Omicron extensively but incompletely escapes Pfizer BNT162b2 neutralization. *Nature* **602**, 654-656 (2022). https://doi.org/10.1038/s41586-021-04387-1

15 Andrews, N. *et al.* Covid-19 Vaccine Effectiveness against the Omicron (B.1.1.529) Variant. *N Engl J Med* **386**, 1532-1546 (2022). https://doi.org/10.1056/NEJMoa2119451

16 Tseng, H. F. *et al.* Effectiveness of mRNA-1273 against SARS-CoV-2 Omicron and Delta variants. *Nat Med* **28**, 1063-1071 (2022). https://doi.org/10.1038/s41591-022-01753-y

17 Gruell, H. *et al.* mRNA booster immunization elicits potent neutralizing serum activity against the SARS-CoV-2 Omicron variant. *Nat Med* **28**, 477-480 (2022). https://doi.org/10.1038/s41591-021-01676-0

18 Wang, Q. *et al.* Alarming antibody evasion properties of rising SARS-CoV-2 BQ and XBB subvariants. *Cell* **186**, 279-286 e278 (2023). https://doi.org/10.1016/j.cell.2022.12.018

1109 19 Scheaffer, S. M. *et al.* Bivalent SARS-CoV-2 mRNA vaccines increase breadth of
1110 neutralization and protect against the BA.5 Omicron variant in mice. *Nat Med* **29**, 247-
1111 257 (2023). https://doi.org/10.1038/s41591-022-02092-8
1112 20 Khoury, D. S. *et al.* Predicting the efficacy of variant-modified COVID-19 vaccine boosters.
1113 *Nat Med* **29**, 574-578 (2023). https://doi.org/10.1038/s41591-023-02228-4
1114 21 Chalkias, S. *et al.* A Bivalent Omicron-Containing Booster Vaccine against Covid-19. *N*
1115 *Engl J Med* **387**, 1279-1291 (2022). https://doi.org/10.1056/NEJMoa2208343
1116 22 Collier, A. Y. *et al.* Immunogenicity of BA.5 Bivalent mRNA Vaccine Boosters. *N Engl J Med*
1117 **388**, 565-567 (2023). https://doi.org/10.1056/NEJMc2213948
1118 23 Davis-Gardner, M. E. *et al.* Neutralization against BA.2.75.2, BQ.1.1, and XBB from mRNA
1119 Bivalent Booster. *N Engl J Med* **388**, 183-185 (2023).
1120 https://doi.org/10.1056/NEJMc2214293
1121 24 Wang, Q. *et al.* Deep immunological imprinting due to the ancestral spike in the current
1122 bivalent COVID-19 vaccine. *Cell Rep Med* **4**, 101258 (2023).
1123 https://doi.org/10.1016/j.xcrm.2023.101258
1124 25 Wang, Q. *et al.* SARS-CoV-2 neutralising antibodies after bivalent versus monovalent
1125 booster. *Lancet Infect Dis* **23**, 527-528 (2023). https://doi.org/10.1016/S1473-
1126 3099(23)00181-0
1127 26 Alsoussi, W. B. *et al.* SARS-CoV-2 Omicron boosting induces de novo B cell response in
1128 humans. *Nature* **617**, 592-598 (2023). https://doi.org/10.1038/s41586-023-06025-4
1129 27 Park, Y. J. *et al.* Imprinted antibody responses against SARS-CoV-2 Omicron sublineages.
1130 *Science* **378**, 619-627 (2022). https://doi.org/10.1126/science.adc9127
1131 28 Carreno, J. M., Singh, G., Simon, V., Krammer, F. & group, P. V. I. s. Bivalent COVID-19
1132 booster vaccines and the absence of BA.5-specific antibodies. *Lancet Microbe* **4**, e569
1133 (2023). https://doi.org/10.1016/S2666-5247(23)00118-0
1134 29 Cobey, S. & Hensley, S. E. Immune history and influenza virus susceptibility. *Curr Opin*
1135 *Virol* **22**, 105-111 (2017). https://doi.org/10.1016/j.coviro.2016.12.004
1136 30 Song, S. *et al.* A systematic review and meta-analysis on the effectiveness of bivalent
1137 mRNA booster vaccines against Omicron variants. *Vaccine* **42**, 3389-3396 (2024).
1138 https://doi.org/10.1016/j.vaccine.2024.04.049
1139 31 Hoffmann, M. A. G. *et al.* ESCRT recruitment to SARS-CoV-2 spike induces virus-like
1140 particles that improve mRNA vaccines. *Cell* (2023).
1141 https://doi.org/https://doi.org/10.1016/j.cell.2023.04.024
1142 32 Hsieh, C. L. *et al.* Structure-based design of prefusion-stabilized SARS-CoV-2 spikes.
1143 *Science* **369**, 1501-1505 (2020). https://doi.org/10.1126/science.abd0826
1144 33 Barnes, C. O. *et al.* SARS-CoV-2 neutralizing antibody structures inform therapeutic
1145 strategies. *Nature* **588**, 682-687 (2020). https://doi.org/10.1038/s41586-020-2852-1
1146 34 Li, C. J. & Chang, S. C. SARS-CoV-2 spike S2-specific neutralizing antibodies. *Emerg*
1147 *Microbes Infect* **12**, 2220582 (2023). https://doi.org/10.1080/22221751.2023.2220582
1148 35 Crawford, K. H. D. *et al.* Protocol and Reagents for Pseudotyping Lentiviral Particles with
1149 SARS-CoV-2 Spike Protein for Neutralization Assays. *Viruses* **12** (2020).
1150 https://doi.org/10.3390/v12050513
1151 36 Robbiani, D. F. *et al.* Convergent antibody responses to SARS-CoV-2 in convalescent
1152 individuals. *Nature* **584**, 437-442 (2020). https://doi.org/10.1038/s41586-020-2456-9

1153 37 Wang, Z. *et al.* Analysis of memory B cells identifies conserved neutralizing epitopes on
1154 the N-terminal domain of variant SARS-Cov-2 spike proteins. *Immunity* **55**, 998-1012
1155 e1018 (2022). https://doi.org/10.1016/j.immuni.2022.04.003
1156 38 Miller, J. *et al.* Substantial Neutralization Escape by SARS-CoV-2 Omicron Variants BQ.1.1
1157 and XBB.1. *N Engl J Med* **388**, 662-664 (2023). https://doi.org/10.1056/NEJMc2214314
1158 39 Feng, S. *et al.* Correlates of protection against symptomatic and asymptomatic SARS-
1159 CoV-2 infection. *Nat Med* **27**, 2032-2040 (2021). https://doi.org/10.1038/s41591-021-
1160 01540-1
1161 40 Fan, C. *et al.* Neutralizing monoclonal antibodies elicited by mosaic RBD nanoparticles
1162 bind conserved sarbecovirus epitopes. *Immunity* **55**, 2419-2435 e2410 (2022).
1163 https://doi.org/10.1016/j.immuni.2022.10.019
1164 41 Fan, C. *et al.* Cross-reactive sarbecovirus antibodies induced by mosaic RBD
1165 nanoparticles. *Proc Natl Acad Sci U S A* **122**, e2501637122 (2025).
1166 https://doi.org/10.1073/pnas.2501637122
1167 42 Starr, T. N. *et al.* Deep Mutational Scanning of SARS-CoV-2 Receptor Binding Domain
1168 Reveals Constraints on Folding and ACE2 Binding. *Cell* **182**, 1295-1310 e1220 (2020).
1169 https://doi.org/10.1016/j.cell.2020.08.012
1170 43 Taylor, A. L. & Starr, T. N. Deep mutational scans of XBB.1.5 and BQ.1.1 reveal ongoing
1171 epistatic drift during SARS-CoV-2 evolution. *PLoS Pathog* **19**, e1011901 (2023).
1172 https://doi.org/10.1371/journal.ppat.1011901
1173 44 Cohen, A. A. *et al.* Mosaic sarbecovirus nanoparticles elicit cross-reactive responses in
1174 pre-vaccinated animals. *Cell* **187**, 5554-5571 e5519 (2024).
1175 https://doi.org/10.1016/j.cell.2024.07.052
1176 45 Greaney, A. J. *et al.* Mapping mutations to the SARS-CoV-2 RBD that escape binding by
1177 different classes of antibodies. *Nat Commun* **12**, 4196 (2021).
1178 https://doi.org/10.1038/s41467-021-24435-8
1179 46 Callaway, H. M. *et al.* Bivalent intra-spike binding provides durability against emergent
1180 Omicron lineages: Results from a global consortium. *Cell Rep* **42**, 112014 (2023).
1181 https://doi.org/10.1016/j.celrep.2023.112014
1182 47 Sanders, R. W. *et al.* A next-generation cleaved, soluble HIV-1 Env trimer, BG505
1183 SOSIP.664 gp140, expresses multiple epitopes for broadly neutralizing but not non-
1184 neutralizing antibodies. *PLoS Pathog* **9**, e1003618 (2013).
1185 https://doi.org/10.1371/journal.ppat.1003618
1186 48 Walls, A. C. *et al.* Structure, Function, and Antigenicity of the SARS-CoV-2 Spike
1187 Glycoprotein. *Cell* **181**, 281-292 e286 (2020). https://doi.org/10.1016/j.cell.2020.02.058
1188 49 Wrapp, D. *et al.* Cryo-EM structure of the 2019-nCoV spike in the prefusion
1189 conformation. *Science* **367**, 1260-1263 (2020). https://doi.org/10.1126/science.abb2507
1190 50 Tan, C. Y. *et al.* Effectiveness of bivalent mRNA vaccines against medically attended
1191 symptomatic SARS-CoV-2 infection and COVID-19-related hospital admission among
1192 SARS-CoV-2-naive and previously infected individuals: a retrospective cohort study.
1193 *Lancet Infect Dis* **23**, 1343-1348 (2023). https://doi.org/10.1016/S1473-3099(23)00373-0
1194 51 Bowen, J. E. *et al.* SARS-CoV-2 spike conformation determines plasma neutralizing
1195 activity elicited by a wide panel of human vaccines. *Sci Immunol* **7**, eadf1421 (2022).
1196 https://doi.org/10.1126/sciimmunol.adf1421

1197 52 Balinsky, C. A. *et al.* Antibodies to S2 domain of SARS-CoV-2 spike protein in Moderna
1198 mRNA vaccinated subjects sustain antibody-dependent NK cell-mediated cell cytotoxicity
1199 against Omicron BA.1. *Front Immunol* **14**, 1266829 (2023).
1200 https://doi.org/10.3389/fimmu.2023.1266829
1201 53 Keeton, R. *et al.* T cell responses to SARS-CoV-2 spike cross-recognize Omicron. *Nature*
1202 **603**, 488-492 (2022). https://doi.org/10.1038/s41586-022-04460-3
1203 54 Rydyznski Moderbacher, C. *et al.* Antigen-Specific Adaptive Immunity to SARS-CoV-2 in
1204 Acute COVID-19 and Associations with Age and Disease Severity. *Cell* **183**, 996-1012
1205 e1019 (2020). https://doi.org/10.1016/j.cell.2020.09.038
1206 55 Muik, A. *et al.* Exposure to BA.4/5 S protein drives neutralization of Omicron BA.1, BA.2,
1207 BA.2.12.1, and BA.4/5 in vaccine-experienced humans and mice. *Sci Immunol* **7**,
1208 eade9888 (2022). https://doi.org/10.1126/sciimmunol.ade9888
1209 56 Ying, B. *et al.* Boosting with variant-matched or historical mRNA vaccines protects
1210 against Omicron infection in mice. *Cell* **185**, 1572-1587 e1511 (2022).
1211 https://doi.org/10.1016/j.cell.2022.03.037
1212 57 Pallesen, J. *et al.* Immunogenicity and structures of a rationally designed prefusion
1213 MERS-CoV spike antigen. *Proc Natl Acad Sci U S A* **114**, E7348-E7357 (2017).
1214 https://doi.org/10.1073/pnas.1707304114
1215 58 McBride, C. E., Li, J. & Machamer, C. E. The cytoplasmic tail of the severe acute
1216 respiratory syndrome coronavirus spike protein contains a novel endoplasmic reticulum
1217 retrieval signal that binds COPI and promotes interaction with membrane protein. *J Virol*
1218 **81**, 2418-2428 (2007). https://doi.org/10.1128/JVI.02146-06
1219 59 Korber, B. *et al.* Tracking Changes in SARS-CoV-2 Spike: Evidence that D614G Increases
1220 Infectivity of the COVID-19 Virus. *Cell* **182**, 812-827 e819 (2020).
1221 https://doi.org/10.1016/j.cell.2020.06.043
1222 60 Miettinen, H. M., Rose, J. K. & Mellman, I. Fc receptor isoforms exhibit distinct abilities
1223 for coated pit localization as a result of cytoplasmic domain heterogeneity. *Cell* **58**, 317-
1224 327 (1989). https://doi.org/10.1016/0092-8674(89)90846-5
1225 61 Pinto, D. *et al.* Broad betacoronavirus neutralization by a stem helix-specific human
1226 antibody. *Science* (2021). https://doi.org/10.1126/science.abj3321
1227 62 Kariko, K. *et al.* Incorporation of pseudouridine into mRNA yields superior
1228 nonimmunogenic vector with increased translational capacity and biological stability.
1229 *Mol Ther* **16**, 1833-1840 (2008). https://doi.org/10.1038/mt.2008.200
1230 63 Kariko, K., Muramatsu, H., Ludwig, J. & Weissman, D. Generating the optimal mRNA for
1231 therapy: HPLC purification eliminates immune activation and improves translation of
1232 nucleoside-modified, protein-encoding mRNA. *Nucleic Acids Res* **39**, e142 (2011).
1233 https://doi.org/10.1093/nar/gkr695
1234 64 Pardi, N. *et al.* Expression kinetics of nucleoside-modified mRNA delivered in lipid
1235 nanoparticles to mice by various routes. *J Control Release* **217**, 345-351 (2015).
1236 https://doi.org/10.1016/j.jconrel.2015.08.007
1237 65 Hsieh, C. L. *et al.* Prefusion-stabilized SARS-CoV-2 S2-only antigen provides protection
1238 against SARS-CoV-2 challenge. *Nat Commun* **15**, 1553 (2024).
1239 https://doi.org/10.1038/s41467-024-45404-x

1240 66 Cohen, A. A. *et al.* Mosaic RBD nanoparticles protect against challenge by diverse
1241 sarbecoviruses in animal models. *Science* **377**, eabq0839 (2022).
1242 https://doi.org/10.1126/science.abq0839
1243 67 Mastronarde, D. N. Automated electron microscope tomography using robust prediction
1244 of specimen movements. *J Struct Biol* **152**, 36-51 (2005).
1245 https://doi.org/10.1016/j.jsb.2005.07.007
1246 68 Punjani, A., Rubinstein, J. L., Fleet, D. J. & Brubaker, M. A. cryoSPARC: algorithms for
1247 rapid unsupervised cryo-EM structure determination. *Nat Methods* **14**, 290-296 (2017).
1248 https://doi.org/10.1038/nmeth.4169
1249 69 Cohen, A. A. *et al.* Mosaic nanoparticles elicit cross-reactive immune responses to
1250 zoonotic coronaviruses in mice. *Science* **371**, 735-741 (2021).
1251 https://doi.org/10.1126/science.abf6840
1252 70 West, A. P., Jr. *et al.* Computational analysis of anti-HIV-1 antibody neutralization panel
1253 data to identify potential functional epitope residues. *Proc Natl Acad Sci U S A* **110**,
1254 10598-10603 (2013). https://doi.org/10.1073/pnas.1309215110
1255 71 Starr, T. N. *et al.* Shifting mutational constraints in the SARS-CoV-2 receptor-binding
1256 domain during viral evolution. *Science* **377**, 420-424 (2022).
1257 https://doi.org/10.1126/science.abo7896
1258 72 Greaney, A. J. *et al.* Comprehensive mapping of mutations in the SARS-CoV-2 receptor-
1259 binding domain that affect recognition by polyclonal human plasma antibodies. *Cell Host*
1260 *Microbe* **29**, 463-476 e466 (2021). https://doi.org/10.1016/j.chom.2021.02.003
1261 73 Hills, R. A. *et al.* Proactive vaccination using multiviral Quartet Nanocages to elicit broad
1262 anti-coronavirus responses. *Nat Nanotechnol* **19**, 1216-1223 (2024).
1263 https://doi.org/10.1038/s41565-024-01655-9
1264 74 Barnes, C. O. *et al.* SARS-CoV-2 neutralizing antibody structures inform therapeutic
1265 strategies. *Nature* **588**, 682-687 (2020). https://doi.org/10.1038/s41586-020-2852-1
1266 75 Landau, M. *et al.* ConSurf 2005: the projection of evolutionary conservation scores of
1267 residues on protein structures. *Nucleic Acids Res* **33**, W299-302 (2005).
1268 https://doi.org/10.1093/nar/gki370
1269 76 Saphire, E. O. *et al.* Crystal structure of a neutralizing human IGG against HIV-1: a
1270 template for vaccine design. *Science* **293**, 1155-1159 (2001).
1271

1272 **Acknowledgements**

1273 We thank J. Vielmetter, A. Lam, and the Caltech Protein Expression Center for assistance
1274 with protein production, S. Chen and the Caltech Cryo-EM facility for cryo-EM data
1275 collection, M. Anaya (Caltech) for a BirA expression plasmid, J.E. Robinson (Tulane
1276 University) for the JR-52 antibody, J. Bloom (Fred Hutchinson Cancer Research Center)
1277 and T. Starr (University of Utah) for RBD libraries, and J. Bloom (Fred Hutchinson) and P.

1278 Bieniasz (Rockefeller University) for neutralization assay reagents. We thank J. Keeffe
1279 for guidance on ELISA method development, A. West for Swift DMS support, Y. Tam
1280 (Acuitas Therapeutics) for careful reading of the manuscript, B. Wold, G. Tolomiczenko,
1281 and the Caltech Merkin Institute for Translational Research for helpful discussions. Cryo-
1282 EM was performed in the Beckman Institute Resource Center for Transmission Electron
1283 Microscopy at Caltech. We thank Labcorp Drug Development–Antibody Reagents and
1284 Vaccines (Denver, PA) (formerly Covance, Inc.) for mouse immunization studies, and
1285 RNAcore (Houston Methodist Research Institute) for synthesis of mRNAs and helpful
1286 discussion. Figures 1A, 1C, and 5A were created with Biorender.com. These studies were
1287 funded by Wellcome Leap (P.J.B.), the National Institutes of Health P01-AI165075 (P.J.B.)
1288 and DP5OD033362 (M.A.G.H), Gates Foundation INV-034638 (P.J.B.) and INV-056219
1289 (M.A.G.H.), the Merkin Institute for Translational Research (Caltech) (P.J.B), and the
1290 George Mason University Fast Grants (P.J.B.). This manuscript is the result of funding in
1291 whole or in part by the National Institutes of Health (NIH). It is subject to the NIH Public
1292 Access Policy. Through acceptance of this federal funding, NIH has been given a right to
1293 make this manuscript publicly available in PubMed Central upon the Official Date of
1294 Publication, as defined by NIH.

1295

1296 **Author contributions**:

1297 Conceptualization: C.F., A.A.C., K.A.D., P.J.B., and M.A.G.H.; Methodology: C.F., A.A.C.,
1298 K.A.D., A.-C.P.F., P.J.B., and M.A.G.H.; Investigation: C.F., A.A.C., K.A.D., A.V.R., A.-
1299 C.P.F., Z.Y., P.N.P.G., K.E.H.T., W.J.M., P.J.C.L., and M.A.G.H.; Writing – original draft:
1300 C.F., A.A.C., K.A.D., P.J.B., and M.A.G.H.; Writing – review and editing: C.F., A.A.C.,

K.A.D., A.-C.P.F., P.J.C.L., P.J.B., and M.A.G.H.; Visualization: C.F., A.A.C., K.A.D.; Supervision: P.J.B., and M.A.G.H.; Funding: P.J.B., and M.A.G.H.

Competing interests

M.A.G.H. and P.J.B. are inventors on a US patent application filed by the California Institute of Technology that covers the EABR technology described in this work. P.J.B. is a scientific advisor for Vaccine Company, Inc. M.A.G.H. is a scientific consultant for Vaccine Company, Inc. W.J.M. and P.J.C.L. are employees of Acuitas Therapeutics, a company developing lipid nanoparticle delivery technology; P.J.C.L. holds equity in Acuitas Therapeutics.

Materials, data, and code availability

Materials generated in this study are available upon request through a Materials Transfer Agreement. Code used for data processing and visualization of DMS results is available upon request. Main text and supplementary data will be publicly available. DMS raw sequencing data will be available under an NCBI SRA. Cryo-EM density maps are deposited in the EMDB with accession codes: EMD-71513, EMD-71514, EMD-71515 and EMD-71516. Materials are available upon request to corresponding authors with a signed material transfer agreement, and other information required to analyze the data in this paper is available from the lead contacts upon request. This paper does not report original code. The work is licensed under a Creative Commons Attribution 4.0 International (CC BY 4.0) license, which permits unrestricted use, distribution, and reproduction in any medium, provided the original work is properly cited. To view a copy of this license, visit

https://creativecommons.org/licenses/by/4.0/. This license does not apply to figures/photos/artwork or other content included in the article that is credited to a third party; obtain authorization from the rights holder before using such material.